Journal of Radiation Research and Applied Sciences 18 (2025) 101879

Contents lists available at ScienceDirect

Journal of Radiation Research and Applied Sciences

journal homepage: www.journals.elsevier.com/journal-of-radiation-research-and-applied-sciences

Significance of thermal radiation in a non-Newtonian (Reiner-Rivlin) model past a cylindrical surface with application in a thermal management system

A.M. Obalalu [a], Ayodeji Felix Isarinade [b], Umair Khan [c,d,**], Aurang Zaib [e], Najiyah Safwa Khashi'ie [f], Dalia H. Elkamchouchi [g,*]

[a] Department of Mathematics and Statistics, Kwara State University, Malete, Nigeria
[b] Department of Mathematics and Data Science, Wigwe University, Isiokpo, Rivers. State, Nigeria
[c] Department of Mathematics, Saveetha School of Engineering, Saveetha Institute of Medical and Technical Sciences, Saveetha University, Chennai, 602105, Tamil Nadu, India
[d] Department of Mathematics, Faculty of Science, Sakarya University, Serdivan/Sakarya, 54050, Turkey
[e] Department of Mathematics, University of Karachi, Karachi, 75270, Pakistan
[f] Fakulti Teknologi dan Kejuruteraan Mekanikal, Universiti Teknikal Malaysia Melaka, Hang Tuah Jaya, Durian Tunggal, 76100, Melaka, Malaysia
[g] Department of Information Technology, College of Computer and Information Sciences, Princess Nourah bint Abdulrahman University, P.O. Box 84428, Riyadh 11671, Saudi Arabia

ARTICLE INFO

Keywords:
Reiner–Rivlin (non-Newtonian) fluid
stagnation point flow
Chebyshev collocation method
thermal radiation
motile microorganisms

ABSTRACT

The study of thermal radiation in fluid mechanics has gained considerable attention due to its pivotal role in heat and mass transfer processes across various industrial and engineering applications. Building on this motivation, this study emphasizes how thermal radiation affects the transport of heat and mass in the flow. Specifically, it explores the stagnation-point flow behavior of a Reiner–Rivlin type non-Newtonian fluid that arises due to a stretching cylindrical surface. The analysis is extended to incorporate bioconvective transport due to motile microorganisms, Soret and Dufour effects, and Joule heating effects. The boundary conditions assume prescribed wall temperature and solute concentration, enabling the derivation of the similarity variables. Curvature effects are introduced through a dimensionless curvature parameter, defined in terms of the inverse of the cylinder radius, which quantifies deviations from a flat plate configuration. This parameter is varied to investigate its impact on the structure of stagnation-point flow and thermal transport. The transformed nonlinear ordinary differential equations are numerically solved using the Chebyshev Collocation method. Validation of the computational results is performed by comparing them with existing solutions under certain limiting cases. The study further investigates the interplay between thermal radiation and microorganism motility, which occurs through the radiation-induced temperature rise influencing bioconvective density gradients and microorganism distribution. Parametric studies are carried out to examine how key factors such as curvature, thermal radiation, bioconvective parameters, diffusion coefficients, and Reiner–Rivlin fluid characteristics affect flow profiles, temperature and concentration distributions, motile microorganism density, and skin friction. The findings reveal that an increase in thermal radiation leads to a rise in temperature distribution and modifies the bio-convective flow field. These insights are vital for optimizing the design of systems involving non-Newtonian fluids in energy, biomedical, and microfluidic applications.

* Corresponding author.
** Corresponding author. Department of Mathematics, Saveetha School of Engineering, Saveetha Institute of Medical and Technical Sciences, Saveetha University, Chennai, 602105, Tamil Nadu, India.
E-mail addresses: adebowale.obalalu17@gmail.com (A.M. Obalalu), isarinadea@gmail.com (A.F. Isarinade), umairkhan@sakarya.edu.tr (U. Khan), zaib20042002@gmail.com (A. Zaib), najiyah@utem.edu.my (N.S. Khashi'ie), dhelkamchouchi@pnu.edu.sa (D.H. Elkamchouchi).

https://doi.org/10.1016/j.jrras.2025.101879
Received 5 July 2025; Received in revised form 7 August 2025; Accepted 11 August 2025
Available online 20 August 2025

Nomenclature

Symbol	Meaning	SI Unit
μ_c	Cross-viscosity parameter	Pars (Pascal-second)
μ_f, ρ_f	Dynamic viscosity and mass density of fluid	Pars, kg/m^3
K_0, Q_0	Chemical reaction and internal heat generation rates	s^{-1}, W/m^3
E_a	Activation energy constant	J/mol
B_0	Applied magnetics flux intensity	T (Tesla)
k_f	Thermal conductivity	$W/(m\cdot K)$
$\widetilde{n}$	Microbial population density	$1/m^3$
D_m	Microorganism motility diffusion rate	m^2/s
$\nu_f = \mu_f/\rho_f$	Kinematic viscosity (momentum diffusivity)	m^2/s
σ_f	Electrical conductivity of the fluid	S/m (Siemens per meter)
$\exp\left(\frac{E_a}{kT}\right)$	Arrhenius temperature function	Dimensionless
$(c_p)_f$	Specific heat at constant pressure	J/(kg.K)
k_T	Thermodiffusion (Soret effect) coefficient	K^{-1}
$\widetilde{n}_\infty$	Ambient microbial concentration (far field)	$1/m^3$
W_c	Peak velocity of microorganism	m/s
Sr	Soret factor	Dimensionless
Du	Dufour factor	Dimensionless
Q	Heat generation parameter	Dimensionless
Pr	Prandtl Number	Dimensionless
S	Suction parameter,	Dimensionless
Ec	Eckert Number	Dimensionless
K	Chemical reaction parameter	Dimensionless
Rd	Thermal radiation parameter	Dimensionless
q_w	Wall heat flux	W/m^2
A	Velocity ratio parameter	Dimensionless
Pe	Peclet (Pe) number	Dimensionless
M	curvature parameter	Dimensionless
Ha	magnetic interaction parameter	Dimensionless
Lb	bioconvective Lewis parameter	Dimensionless
β	Reiner-Rivlin fluid parameter	Dimensionless
Sc	Schmidt Number	Dimensionless
Re_x	local Reynolds number	Dimensionless

1. Introduction

Thermal radiation refers to the emission of electromagnetic radiation from a body due to its temperature. It arises from the random motion of charged particles within matter. The intensity and wavelength distribution of this radiation are determined by both the temperature and the surface properties of the emitting body. Unlike conduction and convection, thermal radiation does not require a medium for transfer. As such, it plays a crucial role in high-temperature environments, vacuum conditions, and radiative heat transfer applications in engineering and astrophysics. This form of heat transfer does not require a medium, making it essential in applications involving high temperatures, vacuum environments, and radiative heat transfer analysis in engineering and astrophysics. Objects naturally release electromagnetic radiation through thermal radiation which originates from their temperature level. Thermal radiation is among three fundamental transfer mechanisms of heat with conduction and convection (Galal et al., 2025a). Thermal radiation stands apart from conduction and convection because it transfers heat through electromagnetic waves without requiring any medium and thus makes it essential in numerous natural and technological applications even in vacuum conditions. The scientific field of thermal radiation started in the early 19th century through work conducted by Wilhelm Stefan and Joseph John Tyndall. The insights that led to radiation being recognized as a quantum phenomenon first occurred when Max Planck conducted his groundbreaking work during the beginning of the twentieth century. This research established essential principles between modern quantum mechanics and thermodynamics (Anjum et al., 2025). Thermal radiation encompasses a wide range of electromagnetic waves, from infrared radiation to visible light and beyond (Khan, Obalalu, et al., 2025). Lower temperature bodies release infrared radiation which gradually shifts to visible spectrum frequencies and then to ultraviolet at higher temperatures (Cao et al., 2025). The intensity of thermal radiation depends on two fundamental factors: temperature and emissivity level of an object. Thermal radiation operates as the critical operational component in the technology industries. Such systems depend on thermal radiation principles to operate as the primary technological component in aerospace applications. To operate successfully in space vacuum satellite and space station temperature control systems need the use of spacecraft radiators as heat release systems (Obalalu, Salawu, et al., 2025). The design process of heat exchangers and power plants and furnaces depends on perfect thermal radiation controls for achieving both operational safety standards and performance efficiency (Eswaramoorthi et al., 2025). Medical professionals use thermal radiation fundamentals to operate infrared pain treatment systems while operating diagnostic instruments that rely on thermal imaging cameras. Various current applications and future technologies benefit from thermal radiation which has led to multiple useful applications across present-day applications and future technological systems (Dou et al., 2025). Galal et al. (Galal et al., 2025b) study the thermal radiation effect on thermo-bioconvection flow due to a ternary hybrid nanoliquid across a sheet that offers the impacts of a heat source by the accompanying thermophoresis impacts. The research emphasized the importance of thermophoretic transport of particles along temperature gradients, which is a significant process in such fields as aerospace, electronic cooling and bio-medical device engineering. Also, the recent work of Gasmi et al. (Gasmi et al., 2025) study the thermal characteristics of trihybrid nanofluid flow over a rotating disk subjected with the effect of local thermal non-equilibriu thermal radiation, gyrotactic microorganisms, porous media, and Marangoni convection. Zheng et al. (Zheng et al., 2024) investigate the potential of a hexagonal ring nanostructure to function as both a solar absorber and a thermal emitter. The results show that the structure is of high-performance in terms of the absorption and radiation and have the potential of being deployed in the field of solar power harvesting, thermal emitters, and other complex photothermal utilization.

The research on deforming cylinders has also gained momentum in recent years, especially since 2020, and has found extensive applications in engineering, biomechanics, fluid-structure interaction and soft robotics (Obalalu, Khan, et al., 2025). Deforming cylinders refer to those structures that deform dynamically either due to the action of external forces, internal loads, thermal gradients or other time-dependent boundary conditions that result in shape change or variation in volume. These deformations may be axial, radial, torsional, or a mixture of the modes. Research on deforming cylinders repeats most of its analysis across solid mechanics followed by material science and structural engineering (Mao et al., 2025). The definition of a cylinder includes parallel straight sides that run throughout its body together with circular forms in its cross-sections. Various forces consisting of tension and torsion and bending reduce essential performance levels of cylinders when deformations occur. Deformation refers to the change in shape or size of an object due to applied forces or environmental conditions. Engineering investigations benefit from theories about cylinder deformation under applied loads because they serve multiple engineering applications and natural science studies. Multiple sectors require cylindrical structures for pipe and shaft production before applying them to civil engineering applications including columns and silos and pressure vessels. Cylindrical body deformation processes depend heavily on four major components that involve material characteristics and load intensity together with the influence of boundary limits and loading varieties (Galal et al., 2025c). External forces cause elastic cylinder deformation hence returning to the original form but leave behind permanent shape changes because of plastic deformations. Engineers who collaborate with designers should grasp elastic and plastic behavior because it provides both safety characteristics and extended operational lifespans to cylindrical structures Aerospace system designs depend on cartilage material because it constitutes crucial elements such as fuel tanks and rocket boosters and fuselages that need high-pressure and heat-resistant materials. Automobile industries require cylindrical components to construct engines and maintain exhaust systems with suspension systems. Better vehicle security and longer lasting performance emerge when engineers achieve successful control and predictions of system deformations in these applications (Imran et al., 2025a). The study of deforming cylinders provides major advantages to the industrial manufacturing sector. Cylindrical materials undergo changes to both their external appearance and internal substance through force application throughout extrusion and rolling and forging processes (Hussain et al., 2025). The comprehension of deformation processes by manufacturers serves their goal to reach maximum production efficiency while minimizing waste and developing top-quality end products. Cylinder deformation stands as a primary technology in the field of energy management. Research of pressure-induced along with force-induced deformation mechanisms in cylindrical pipes during pipeline development becomes vital for preventing system breakdowns (Kumari et al., 2025). Deforming cylinders play an important role in the study of biological systems which includes blood vessels and plant stems that support mechanical stresses and strains in cylindrical structures. Structures containing cylindrical shapes show functional modifications when strained because they affect the dynamics of blood flow and patterns of plant expansion (Aich et al., 2025). Cylindrical body deformation ability enables scientists to advance both theoretical study and practical application while improving engineering structures and optimizing production and natural process evaluation. The evolution of technology enables new assessment methods and modification approaches for these deformations so they become more applicable in contemporary engineering and scientific disciplines. The recent work of Yang et al. (Yang et al., 2025) explore a new technique of production of thin-walled hydrogen storage cylinders full active counter-roller spinning (FACRS) of cylinders. The research provides valuable knowledge on the texture development and deformation processes, which shows FACRS as a potential alternative of conventional spinning over mandrel of hydrogen bottles liner. Cham et al. (Cham & Mustafa, 2024) describe an elaborate numerical study of an axial fluid motion forced by deforming cylinder or plate in partial slip and viscoelastic settings. The authors investigate skin friction coefficients and rates of heat transfer over several parameters of the second-grade fluids having used a powerful numerical routine. Jamshidi et al. (Jamshidi & Arefi, 2024) examine the mechanical behavior of cylindrical shells made of functional graded porous materials (FGPMs), whereby three distributions are placed under investigation in terms of porosity, namely monotonous, non-symmetric and symmetric distributions.

Reiner Rivlin model is a mathematical model in fluid mechanics, applicable to the behavior of non-Newtonian liquids, especially, viscoelastic materials. In contrast to Newtonian fluids models where stress is proportional to the strain rate, the ReinerRivlin model supports nonlinear stress strain behavior hence its application to more complex fluids like polymers, slurries and some biological fluids (Mohammed et al., 2023). Scientists developed the Reiner–Rivlin model during the middle period of the twentieth century as an extension theory for fluid mechanics to study complex materials. The viscoelastic nature of a substance exists when flow occurs through viscosity while the material reverts its original form because of its elastic qualities. Material science benefits from this specific property because the model emphasizes it for its crucial role (Galal et al., 2025d). Time-dependent responses together with material recovery between stresses can be properly represented by the Reiner–Rivlin model's mathematical structure which makes it a significant achievement in rheological research. The stress level in Reiner–Rivlin model operates based on the current deformation rates which measure how fast the system stretches or shrinks along with the elastic capabilities of the fluid (Rauf et al., 2025). The model enables memory effects because fluid performance depends on current conditions in combination with its previous deformation behaviors. When adding memory effects through complex modeling approaches the outcomes differ from simple modeling systems which generate immediate force output. The Reiner–Rivlin model gained its importance because it creates accurate fluid descriptions of materials beyond Newtonian fluids. Through the Reiner–Rivlin model researchers can achieve fundamental scientific insights into polymers solutions as well as liquid crystals and biological fluids and industrial materials displaying mixed liquid-solid characteristics (Ogunsanwo et al., 2025). Scientist uses this model to study viscoelastic movement of lava flows and other natural phenomena involving such behavior patterns. Research-based rheological understanding enables scientists to estimate material movements that helps improve natural disaster risk reduction while developing earthquake-resistant structures (Muhammad & Haider, 2025). Imran et al. (John & Aderemi, 2023). investigated how thermodiffusion, bioconvection, and viscous dissipation influence the transport of heat and mass. Their study focused on the bioconvective flow of a non-Newtonian Reiner–Rivlin fluid near the stagnation point over a stretching cylindrical surface. It combines the analyses of entropy generation in order to determine the irreversibility of transport processes. Shoaib et al. (Shoaib et al., 2025a) examined the effects of Soret and Dufour mechanisms on entropy generation in a two-dimensional magnetohydrodynamic (MHD) flow of a Reiner–Rivlin fluid. In their study, they applied artificial intelligence techniques to analyze and evaluate the behavior of the flow system. The article shows the advantages of neural network-based methods in the solution of complicated thermofluid problems and optimization of the temperatures and flows of non-Newtonian fluids. Abhijith et al. (Abhijith et al., 2025) study the flow behaviour of the Reiner-Rivlin nanofluid on inclined flat plate, which includes the effect of magnetic field and quadratic thermal radiation and buoyancy forces.

A stagnation point is a point in a fluid flow at which a fluid has zero velocity relative to the surface or body. When the fluid reaches this point, it stops completely, because of an obstruction, the leading edge, a solid surface, or a bluff body in the flow (Anwar, 2025a; Zeb et al., 2025). In the case of airflow over an aircraft or a sphere, there are commonly stagnation points at the leading edge of the object, where the fluid first encounters the object. At this point, the kinetic energy of flow changes into pressure energy according to the principle of Bernoulli. The analysis of stagnation points is critical in analyses of design nozzles, heat exchangers, wings and spaceships where great importance is attached to the prediction of pressure loads and thermal loads (Khan, Ahmad, et al., 2025). Heat energy develops entirely from fluid kinetic energy because of the friction that occurs between the layers. Stagnation points display significant roles as they control the conversion of key fluid dynamics that take place within these regions (Galal et al., 2025e). A fluid's contact interactions with obstacles depend on the occurrence of points where fluids become stagnant. The boundary conditions produced by multiple engineering processes and natural and atmospheric systems produce stagnation point formation. Surface airflow results in an aircraft nose stagnation point because the airspeed becomes zero within that region. The application of aerodynamic evaluation depends on stagnation points because these points provide the necessary data for calculating body-force distributions in mobile objects (Xu et al., 2025). Stagnation points are frequently calculated in steady incompressible fluid flows since these critical points contain important attributes that emerge during rapid compressible flight of aircraft and rockets. The amount of temperature change in stagnant fluid during compression becomes significant due to total conversion of kinetic energy into internal energy. Engineers use stagnation points as their main heat dissipation element when designing spacecraft systems because these temperature effects are employed in various applications involving space heat shields (Obalalu et al., 2024). The investigation of boundary layers and flow separation within turbulent flow requires the stagnation point to serve as the main reference system (Abbas et al., 2024). Near-stagnation fluid movements assist scientists in discovering turbulence controls and flow separation principles that enhance wing and turbine system functionality.

A bioconvective flow develops when biological organisms come into contact with their surrounding fluid medium resulting in macroscopic movement patterns which stem from the organisms' motion. The organisms move through their fluid environment by swimming or drifting actions which generates flow according to the fluid characteristics (Imran et al., 2025b). Bioconvection describes the collective movement from distinct biological agents producing major flow structures through these agents' coordinated activities. The collective behavior of these microorganisms with fluids creates various structures and vortex-like formation that produces distinctive non-convective flow patterns from biological movements and organism activities (Shoaib et al., 2025b). Bioconvective flows naturally occur in various environmental and biological contexts. Scientific evidence indicates that microbial aggregations, such as plankton colonies, represent one of the earliest natural examples observed in aquatic environments. The cellular propulsion systems of flagella or cilia generate different patterns of organismal motion when organisms move independently through upwelling motions and form vortex structures and convection rolls. The movements spread from aquatic environments down to sediment layers and microbial biofilms while preserving their presence in particular biomaterials (Oyoru & John, 2022). Microorganisms react to environmental gradients through density changes that create different fluid movements from cyclic to oscillatory and other types. The study of bioconvective flows demands combination between fluid mechanics and biological knowledge and physics expertise. Bioconvective flow provides scientific fields with necessary knowledge about microorganism molecular movement patterns because it studies environmental influence at various scales. Natural biological environments use such flowing mechanisms to direct nutrient transportation and waste elimination processes and determine whether a population will cluster or occupy the entire habitat. The combination of planktonic species in aquatic environments leads to bioconvective processes that regulate how nutrients are distributed among different water depths which affects aquatic food systems. Bioconvection enhances nutrient and gas mixing operations in stratified water bodies by acting as their principal mixing process (Gull et al., 2024). The biomedical engineering and biotechnology field requires bioconvective flows to optimize and enhance bioreactor design and development. Biological process effectiveness along with nutrient delivery performances and waste removal functions directly respond to changes in microorganism behavior in such systems. Police-based convective processes reveal potential uses for creating new drug delivery methods by improving the targeted motion of pharmaceutical agents (Li et al., 2025). Environmental science benefits from bioconvection research that shows the connection between sediment transport methods and pollutant dissipation together with aquatic organism behavior thus enhancing water body management procedures. Venkatadri et al. (Venkatadri et al., 2025) explore the natural magnetohydrodynamic (MHD) triple convection flow of electrically conducting water with oxytactic microorganism and electromagnetic microbial fuel cells. Sowayan et al. (Sowayan et al., 2025) explore the heat and mass transfer properties of a Jeffrey nanofluid having microorganisms passing a porous and two directional moving boundaries. The experiment investigates the effect of prescribed surface temperature (PST) as well as prescribed heat flux (PHF) systems. ATSS model based upon applications of Cattaneo-Christov thermal analysis for entropy optimized ternary nanomaterial flow with homogeneous-heterogeneous chemical reactions were study by (Razaq et al., 2023). Modified thermal and solutal fluxes through convective flow of Reiner-Rivlin material were study by (Khan, Razaq, et al., 2023). HARK formulation for entropy optimized convective flow beyond constant thermophysical properties were study by (Hayat, Alsaedi, et al., 2024). KHA model comprising MoS 4 and CoFe 2 O 3 in engine oil invoking non-similar Darcy–Forchheimer flow with entropy and Cattaneo–Christov heat flux were study by (Khan, Hayat, & Alsaedi, 2023). SAT formulation for entropy generated hybrid nanomaterial flow: modified Cattaneo-Christov analysis were study by (Khan et al., 2024). TASA formulation for nonlinear radiative flow of Walter-B nanoliquid invoking microorganism and entropy generation were study by (Hayat, Razzaq, et al., 2024). Impact of bioconvection on the free stream flow of a pseudoplastic nanofluid past a rotating cone are study by (Puneeth et al., 2022). Heat transfer in MHD convective stagnation point flow over a stretching surface with thermal radiations are study by (Anwar, 2025b). Fractional calculus approach for the phase dynamics of Josephson junction are study by (Ali et al., 2021). Numerical analysis of nonlinear time-fractional fluid models for simulating heat transport processes in porous medium are study by (Khan, Rasheed, & Anwar, 2023). Investigation of heat transfer characteristics in MHD hybrid nanofluids with variable viscosity and thermal radiations are study by (Anwar et al., 2025). Heat transfer optimization through viscous ternary nanofluid flow over a stretching/shrinking thin needle are study by (Yu et al., 2025). Numerical study of nonlinear thermal radiation and Joule heating on MHD bioconvection Carreau nanofluid with gyrotactic microorganism are study by (Irfan et al., 2025). A novel exploration of magnetized nano Jeffrey fluid flow over a chemically reacted permeable disk with ohmic heating are study by (Dharmaiah & Shankar Goud, 2025). A study of hybrid nano Ag-MgO-H2O flow fluid past a slim needle with thermal radiation and Neild's boundary re study by (Dharmaiah et al., 2025). Influence of activation energy in steady state hydro dynamic non-Newtonian nano fluid with mobile microorganisms are study by (Dharmaiah et al., 2024). Flow over a stretchable cylinder with nonlinear heat sources/sinks: magnetic dipoles application are study by (Goud et al., 2024). Numerical analysis of heat and mass transfer with viscous dissipation, Joule dissipation, and activation energy are study by (Dharmaiah et al., 2023). Role of Joule heating and activation energy on MHD heat and mass transfer flow in the presence of thermal radiation are study by (Shankar Goud & Dharmaiah, 2023). Numerical solutions for thermal and solutal transport of Jeffrey fluid flow subject to rotation via Keller–Box method are study by (Sarfraz & Muhammad, 2025). Synergistic effects of cadmium telluride and graphite nanoparticles with entropy analysis through Keller-box method are study by (Sarfraz, Muhammad, Ahammad, & Elseesy, 2025). Regression analysis of squeezing-induced hybrid nanofluid flow in Darcy-Forchheimer porous medium are study by (Muhammad & Sarfraz, 2025). Heat and mass transfer analysis in flow of Walter's B nanofluid: A numerical study of dual solutions are study by (Sarfraz, Muhammad, Alrihieli, & Abdelmohimen, 2025). Modulation of energy transport in stagnation point flows involving hybrid nanofluids are study by (Sarfraz & Muhammad, 2024). Significance of Brownian diffusion and thermophoresis in energy and mass optimization for Newtonian and Non-Newtonian fluid flow are study by (Muhammad, Sarfraz, Alrihieli, & Elseesy, 2025). Optimization of energy transport via electro-thermal hybrid nanofluid in parallel disks: A Keller-Box simulation are study by (Muhammad, Sarfraz, Ebaid, & Elmannai, 2025). The unconditionally stable Chebyshev finite-difference time-domain method using piecewise calculation scheme was investigated by (Huang et al., 2025).

1.1. Statement of the problem

In numerous industrial and biomedical applications, such as heat exchangers, bioreactors, and drug delivery systems, fluid flow behavior near curved surfaces plays a crucial role in determining system efficiency and performance. Traditional Newtonian fluid models often fail to accurately represent the complex rheological characteristics encountered in such scenarios, especially when dealing with non-Newtonian fluids like Reiner–Rivlin fluids. Additionally, the presence of microorganisms and bioconvective phenomena, along with thermal and solutal gradients, further complicates the analysis. Despite the importance of understanding these interactions, there exists a lack of detailed studies that couple bioconvection, thermo-diffusion, and Joule heating within non-Newtonian stagnation-point flows near curved geometries. This research addresses this gap by exploring the behavior of Reiner–Rivlin fluids near a stretching cylindrical surface, incorporating key thermal and mass transport mechanisms to enhance the predictive modeling of such systems.

1.2. Aim and objectives of the study

This study aims to analyze the stagnation-point bioconvective flow of a Reiner–Rivlin non-Newtonian fluid over a stretching cylindrical surface by incorporating the effects of Soret/Dufour, Joule heating, chemical reaction and activation energy, Lorentz forces and bioconvection induced by motile microorganisms. To achieve this goal, several objectives are pursued. First, a mathematical model is developed to describe the boundary layer flow of the Reiner–Rivlin fluid while accounting for thermal, solutal, and bioconvective effects. Second, the transformed governing equations are numerically solved using the Chebyshev collocation method to examine the behavior of velocity, temperature, concentration, and microorganism density profiles. Third, the influence of key physical parameters such as curvature, Prandtl number, and bioconvection parameters on the flow and thermal fields are investigated.

2. Mathematical formulation of the flow problem

Consider the steady two-dimensional axisymmetric stagnation-point flow of a Reiner–Rivlin fluid towards a permeable stretchable cylindrical surface. The axial coordinate $\check{x}$ is aligned along the surface of the cylinder, while the radial coordinate $\check{r}$ is normal to it. The flow is assumed to be driven by the stretching of the cylindrical surface and stagnation effects, which are common in processes involving extrusion, polymer processing, and bio-transport. To model the thermal and solutal transport in such systems, we incorporate the effects of thermal radiation, Joule heating, and bioconvection due to motile microorganisms. The linear velocity of the stretching surface is modeled as:

$$\check{u}_s(\check{x}) = u_0\frac{\check{x}}{L}, \tag{1}$$

where u_0 and L denote the positive constant velocity and characteristic length scale, respectively. Therefore, the velocity component in the external (distant) flow field is defined as:

$$\check{u}_e(\check{x}) = u_1\frac{\check{x}}{L}, \tag{2}$$

where u_1 is called the positive constant velocity. In addition, the surface temperature $\check{T}_s(\check{x})$ and surface concentration $\check{C}_s(\check{x})$ on the cylindrical wall are given as follows:

$$\check{T}_s(\check{x}) = \check{T}_\infty + \check{T}_0\left(\frac{\check{x}}{L}\right)^2,\ \check{C}_s(\check{x}) = \check{C}_\infty + \check{C}_0\left(\frac{\check{x}}{L}\right)^2 \tag{3}$$

where $\check{T}_0$ and $\check{C}_0$ are the positive constant temperature and concentration, and $\check{T}_\infty$, and $\check{C}_\infty$ are the ambient temperature and concentration, respectively. In addition, the wall surface microorganism $\check{n}_s(\check{x})$ is defined as:

$$\check{n}_s(\check{x}) = \check{n}_\infty + \check{n}_0\left(\frac{\check{x}}{L}\right)^2 \tag{4}$$

where $\check{n}_\infty$ and $\check{n}_0$ correspond the constant ambient and reference microorganisms, respectively.

Furthermore, Fig. 1a display the flow configuration of the problem. The stress tensor for an inelastic Reiner–Rivlin fluid in index form is defined as (Reiner, 1945):

$$\tau_{ij} = -p\delta_{ij} + \mu_f e_{ij} + \mu_c e_{ik}e_{kj}\ ;\ e_{jj} = 0, \tag{5}$$

in which τ_{ij} stands for the stress tensor, μ_f is the viscosity coefficient, p is the pressure, μ_c is the coefficient of cross viscosity, δ_{ij} is the Kronecker

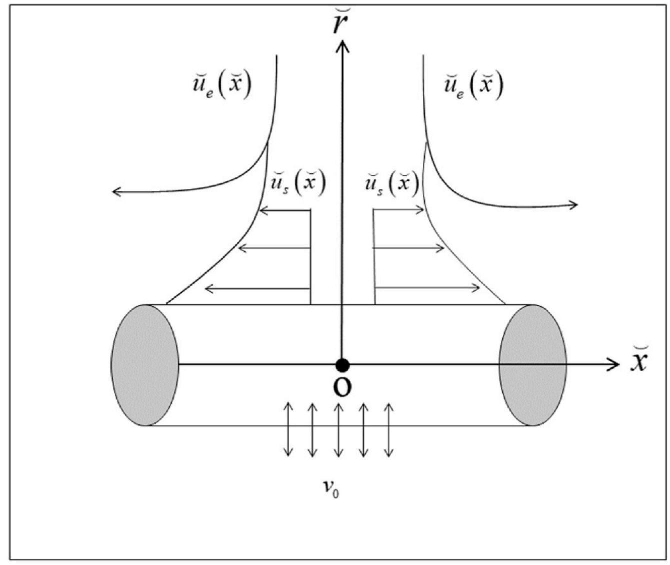

Fig. 1a. Flow configuration of the problem.

symbol and $e_{ij} = \frac{1}{2}\left(\frac{\partial u_i}{\partial x_j} + \frac{\partial u_j}{\partial x_i}\right)$ is the deformation rate tensor. In addition, the stress tensor for an inelastic Reiner–Rivlin fluid in vector form as:

$$\tau = -p\boldsymbol{I} + \mu_f\boldsymbol{e} + \mu_c\boldsymbol{e}\cdot\boldsymbol{e} \tag{6}$$

Here, $\boldsymbol{I}$ is the identity tensor, p is the pressure (scalar), μ_f is the dynamic viscosity (Newtonian part), μ_c is the material parameter for non-linearity and $\boldsymbol{e} = \frac{1}{2}\left((\nabla\boldsymbol{V}) + (\nabla\boldsymbol{V})^T\right)$ is the rate of strain tensor. The equation (6) or Cauchy stress tensor for the Reiner-Rivlin (non-Newtonian) fluid can be written in terms of the first Rivlin-Erickson tensor as:

$$\tau = -p\boldsymbol{I} + \frac{\mu_f}{2}\boldsymbol{A_1} + \frac{\mu_c}{4}\boldsymbol{A_1}\cdot\boldsymbol{A_1} \tag{7}$$

where $\boldsymbol{A_1} = (\nabla\boldsymbol{V}) + (\nabla\boldsymbol{V})^T$ stands for the first Rivlin-Erickson tensor. On the right-hand side of equation (7), the first term represents the isotropic pressure component, second term linear viscous stress, and the third term represents nonlinear quadratic contribution due to rate of deformation.

Using the fundamental conservation laws for incompressible, unsteady, two-dimensional flow of a non-Newtonian (Reiner-Rivlin) model conveying microorganisms, heat and mass transfer along with other distinct physical effects are given in vector notation as follows:

$$\nabla\cdot\boldsymbol{V} = 0 \tag{8}$$

$$\rho_f\left(\frac{\partial\boldsymbol{V}}{\partial t} + (\boldsymbol{V}\cdot\nabla)\boldsymbol{V}\right) = \nabla\cdot\tau + \boldsymbol{J}\times\mathbf{B} + \mathbf{F_t} \tag{9}$$

$$(\rho c_p)_f\left(\frac{\partial\check{T}}{\partial t} + (\boldsymbol{V}\cdot\nabla)\check{T}\right) = k_f\nabla^2\check{T} + \frac{k_T D_T}{c_p c_s}\nabla^2\check{C} + Q^* + \frac{\sigma_f}{\rho_f}\|\boldsymbol{B}\times(\boldsymbol{V_e} - \boldsymbol{V})\|^2 - \nabla\cdot\mathbf{q_r} \tag{10}$$

$$\frac{\partial\check{C}}{\partial t} + (\boldsymbol{V}\cdot\nabla)\check{C} = D_B\nabla^2\check{C} + \frac{k_T D_T}{T_m}\nabla^2\check{T} - R\left(\check{T},\check{C}\right) \tag{11}$$

$$\frac{\partial\check{n}}{\partial t} + (\boldsymbol{V}\cdot\nabla)\check{n} = D_m\nabla^2\check{n} - \nabla\cdot(\check{n}\boldsymbol{V}_c) \tag{12}$$

Here, t is the time, $\boldsymbol{V}$ is the velocity field vector**,** $\boldsymbol{J}$ is the current density, $\boldsymbol{B}$ is the magnetic field vector, ∇ is the differential operator, $\boldsymbol{F_t}$ is the triple diffusive mixed convection, $\check{T}$ is the temperature of the fluid,

k_T is the ratio of thermal diffusion, c_s is the nanoparticle concentration susceptibility, T_m is the fluid mean temperature, Q^* is the heat source/sink term, $\mathbf{q_r}$ is the thermal radiative heat flux vector, $\sigma_f \|\boldsymbol{B} \times (\boldsymbol{V_e} - \boldsymbol{V})\|^2$ is the joule heating with stagnation point velocity, $\check{C}$ is the concentration of the fluid, D_B is the Brownian motion coefficient, D_T is the Thermophoresis coefficient, $R\left(\check{T}, \check{C}\right)$ is the chemical reaction rate with activation energy, $\check{n}$ is the concentration of motile microorganism, D_m is the diffusion coefficient of microorganism and $\boldsymbol{V}_c$ is the swimming velocity vector of microorganism. For the simplification of the given model the following requisite assumptions are employed as:

- Steady flow
- Incompressible flow
- Stagnation-point flow
- Triple-diffusive mixed convection flow
- Non-Newtonian (Reiner-Rivlin) model
- Magnetohydrodynamics
- Heat source/sink effects
- Joule heating and thermal radiation effects
- Soret and Dufour effects
- Chemical reaction and activation energy
- Motile-microorganisms
- Boundary-layer approximations
- Boussinesq approximation

Using the aforementioned assumptions, the leading PDE equations that govern the behavior of the boundary layer flow problem are as follows (Eswaramoorthi et al., 2025):

$$\frac{\partial}{\partial \check{x}}(\check{u}\check{r}) + \frac{\partial}{\partial \check{r}}(\check{v}\check{r}) = 0 \tag{13}$$

$$\check{u}\frac{\partial \check{u}}{\partial \check{x}} + \check{v}\frac{\partial \check{u}}{\partial \check{r}} = \frac{\mu_f}{\rho_f}\left(\frac{\partial^2 \check{u}}{\partial \check{r}^2} + \frac{\partial \check{u}}{\partial \check{r}}\frac{1}{\check{r}}\right) + 2\frac{\mu_c}{\rho_f}\left\{\left(\frac{\partial \check{v}}{\partial \check{r}} + \frac{\partial \check{u}}{\partial \check{x}}\right)\left(\frac{\partial^2 \check{u}}{\partial \check{r}^2} + \frac{\partial \check{u}}{\partial \check{r}}\frac{1}{\check{r}}\right) + \left(\frac{\partial^2 \check{v}}{\partial \check{r}^2} + 2\frac{\partial^2 \check{u}}{\partial \check{x}\partial \check{r}}\right)\frac{\partial \check{u}}{\partial \check{r}}\right\} - \frac{1}{\rho_f}g\left[(1 - C_f)\rho_f\beta^*\left(\check{T} - \check{T}_\infty\right) - \left(\check{C} - \check{C}_\infty\right)(\rho_p - \rho_f) - (\rho_m - \rho_f)\left(\check{n} - \check{n}_\infty\right)\gamma\right], + \left(\check{u}_e - \check{u}\right)\frac{\sigma_f}{\rho_f}B_0^2 + \check{u}_e\frac{d\check{u}_e}{d\check{x}} \tag{14}$$

$$\check{u}\frac{\partial \check{T}}{\partial \check{x}} + \check{v}\frac{\partial \check{T}}{\partial \check{r}} = \frac{k_f}{(\rho c_p)_f}\left(\frac{\partial \check{T}}{\partial \check{r}}\frac{1}{\check{r}} + \frac{\partial^2 \check{T}}{\partial \check{r}^2}\right) + \frac{16\sigma^* \check{T}_\infty^3}{3k^*(\rho c_p)_f}\frac{\partial^2 \check{T}}{\partial \check{r}^2} + \frac{k_T D_T}{c_p c_s}\left(\frac{\partial^2 \check{C}}{\partial \check{r}^2} + \frac{\partial \check{C}}{\partial \check{r}}\frac{1}{\check{r}}\right) + \frac{1}{(\rho c_p)_f}\left(\left(\check{u}_e - \check{u}\right)^2 B_0^2\sigma_f + Q_0\left(\check{T} - \check{T}_\infty\right)\right) \tag{15}$$

$$\check{u}\frac{\partial \check{C}}{\partial \check{x}} + \check{v}\frac{\partial \check{C}}{\partial \check{r}} = D_B\left(\frac{\partial^2 \check{C}}{\partial \check{r}^2} + \frac{\partial \check{C}}{\partial \check{r}}\frac{1}{\check{r}}\right) + \frac{k_T D_T}{T_m}\left(\frac{\partial^2 \check{T}}{\partial \check{r}^2} + \frac{\partial \check{T}}{\partial \check{r}}\frac{1}{\check{r}}\right) - K_0\left(\check{C} - \check{C}_\infty\right)\exp\left(-\frac{E_a}{k\check{T}}\right) \tag{16}$$

Table 1
The mathematical symbol and their description.

Symbol	Meaning	SI Unit
μ_c	Cross-viscosity parameter	Pars (Pascal-second)
μ_f, ρ_f	Dynamic viscosity and mass density of fluid	Pars, kg/m^3
K_0, Q_0	Chemical reaction and internal heat generation rates	$s^{-1}, W/m^3$
E_a	Activation energy constant	J/mol
B_0	Applied magnetic field strength	T (Tesla)
D_T	Thermophoresis diffusion coefficient	m^2/s
$\check{n}$	Concentration of motile microorganism	$1/m^3$
D_m	Microorganism motility diffusion rate	m^2/s
$\nu_f = \mu_f/\rho_f$	Kinematic viscosity (momentum diffusivity)	m^2/s
D_B	Brownian diffusion coefficient	m^2/s
σ_f	Electrical conductivity of the fluid	S/m (Siemens per meter)
$\exp\left(-\frac{E_a}{kT}\right)$	Arrhenius temperature function	Dimensionless
$(c_p)_f$	Specific heat at constant pressure	J/(kg.K)
k_T	Thermodiffusion (Soret effect) coefficient	K^{-1}
$\check{n}_\infty$	Ambient microbial concentration (far field)	$1/m^3$
W_c	Peak velocity of microorganism	m/s

$$\check{u}\frac{\partial \check{n}}{\partial \check{x}} + \check{v}\frac{\partial \check{n}}{\partial \check{r}} = -\frac{bW_c}{\left(\check{C}_s - \check{C}_\infty\right)}\left[\frac{\partial}{\partial \check{r}}\left(\check{n}\frac{\partial \check{C}}{\partial \check{r}}\right)\right] + D_m\left(\frac{\partial^2 \check{n}}{\partial \check{r}^2} + \frac{\partial \check{n}}{\partial \check{r}}\frac{1}{\check{r}}\right) \tag{17}$$

Based on the assumptions of impermeability and the no-slip condition, the corresponding boundary conditions are defined as follows:

Table 2
Dimensionless parameters.

Definition	Description	Definition	Description
$Sr = \dfrac{k_T D_T\left(\breve{T}_s - \breve{T}_\infty\right)}{(C_s - C_\infty)T_m \nu_f}$, $Du = \dfrac{k_T D_T\left(\breve{C}_s - \breve{C}_\infty\right)}{(T_s - T_\infty)c_p c_s \nu_f}$	Soret and Dufour parameters	$A = \dfrac{u_1}{u_0}$	Velocity ratio parameter
$Q = \dfrac{LQ_0}{c_p u_f \rho_f}$	Heat generation parameter	$Pe = \dfrac{W_c b}{D_m}$	Peclet number (Pe)
$\Pr = \dfrac{c_p u_f}{k_f}$	Prandtl number	$M = \sqrt{\dfrac{L\nu_f}{u_0 R^2}}$	Curvature parameter
$S = v_0\sqrt{\dfrac{L}{u_0 \nu_f}}$	Suction parameter,	$Ha = \sqrt{\dfrac{L\sigma_f B_0^2}{u_0 \rho}}$	Magnetic interaction parameter
$Ec = \dfrac{u_0^2}{c_p \breve{T}_0}$	Eckert Number	$Lb = \dfrac{\nu_f}{D_m}$	Bioconvective Lewis
		$\alpha = \left(\breve{T}_s - \breve{T}_\infty\right)/\breve{T}_\infty$	
$K = \dfrac{LK_0}{u_0}$	Chemical reaction parameter	$\beta = \dfrac{\mu_c u_0}{\mu_f L}$	Reiner-Rivlin parameter
$\mathrm{Rd} = \dfrac{4\sigma^* \breve{T}_\infty^3}{k^* k_f}$	Thermal radiation	$Sc = \dfrac{\nu_f}{D_B}$	Schmidt number
$q_w = -k_f\left(\dfrac{\partial \breve{T}}{\partial r}\right)_{r=R}$	Wall heat flux	$Re_x = u_s \breve{x}/\nu_f$	Local Reynolds number

$$\breve{r} = R : \breve{u} = \frac{u_0 \breve{x}}{L}, \breve{v} = -v_0, \breve{T} = \breve{T}_\infty + \breve{T}_0\left(\frac{\breve{x}}{L}\right)^2, \breve{C} = \breve{C}_\infty + \breve{C}_0\left(\frac{\breve{x}}{L}\right)^2,$$
$$\breve{n} = \breve{n}_\infty + \breve{n}_0\left(\frac{\breve{x}}{L}\right)^2, \ \breve{r}\to\infty : \breve{u}\to\breve{u}_e(\breve{x}) = \frac{u_1\breve{x}}{L}, \breve{T}\to\breve{T}_\infty, \breve{C}\to C_\infty, \breve{n}\to\breve{n}_\infty \tag{18}$$

Equation (18) incorporates the assumption of no slip conditions for both thermal and solutal fields, despite variations in surface temperature, motile cell concentration, and solute distribution. Additionally, a constant suction velocity is applied along the surface of the cylinder. The cylinder is considered to stretch axially within its own plane at a linearly increasing velocity, assuming no wall slip occurs. Table 1 display of symbols and their corresponding meanings used in the existing study.

The solutions to equation (14)–(17), subject to the boundary conditions defined in Eq. (18), are obtained by applying the similarity transformations as follows:

$$\vartheta = \frac{\breve{r}^2 - R^2}{2R}\sqrt{\frac{u_0}{L\nu_f}}, \breve{u} = \frac{u_0\breve{x}}{L}p'(\vartheta), \breve{v} = -\frac{R}{\breve{r}}\sqrt{\frac{\nu_f u_0}{L}}p(\vartheta), \chi(\vartheta) = \frac{\breve{T} - \breve{T}_\infty}{\breve{T}_s - \breve{T}_\infty}\ \phi(\vartheta) = \frac{\breve{C} - \breve{C}_\infty}{\breve{C}_s - \breve{C}_\infty}, \xi(\vartheta) = \frac{\breve{n} - \breve{n}_\infty}{\breve{n}_s - \breve{n}_\infty} \tag{19}$$

By using the similarity variables (19), the continuity equation (13) is directly satisfied while the rest of the governing equations (14)–(17) are reformulated into the following transformed expressions as follow:

$$(1 + 2\vartheta M)p''' + 2Mp'' + pp'' - p'^2 + (A - p')Ha^2 + A^2 + \alpha(\chi - Nr\phi - Nc\xi) + 2\beta\{p''^2(1 + 2M\vartheta) + p'p''M + Mp'''p\} = 0 \tag{20}$$

$$\chi''(1 + Rd)2M\vartheta + 2M\chi' + Q\chi + \Pr\left(p\chi' - 2p'\chi + (A - p')^2 Ha^2 Ec\right) + \mathrm{DuPr}(\phi''(1 + 2M\vartheta) + 2M\phi') = 0 \tag{21}$$

$$\phi''(1 + 2M\vartheta) + 2\phi' M + ScSr\{\chi''(1 + 2M\vartheta) + 2\chi' M\} - Sck\phi \exp\left(-\frac{E}{(1 + \delta_0\chi)}\right) + Sc(p\phi' - 2p'\phi) = 0 \tag{22}$$

$$\xi''(1 + 2M\vartheta) + Lb\xi' M - Pe(\phi'\xi' + \phi''\xi + \sigma\phi'') = 0 \tag{23}$$

along with

$$\vartheta = 0 : \mathrm{p}(\vartheta) = S, p'(\vartheta) = 1, \chi(\vartheta) = 1, \phi(\vartheta) = 1, \xi(\vartheta) = 1, \vartheta\to\infty : p'(\vartheta)\to A, \chi(\vartheta)\to 0, \phi(\vartheta)\to 0, \xi(\vartheta)\to 0 \tag{24}$$

Table 2 displays **the key dimensionless parameters used in the above similarity equations.**

It is important to note that the surface velocity of the stretching cylinder exceeds the ambient fluid velocity at $u_0 > u_1$. As a result, $p''(0) < 0$, indicating that $p'(\vartheta)$, which represents the axial velocity profile, is a decreasing function with respect to ϑ. The expressions for the skin friction coefficient, rate of heat transfer (Nusselt number), Sherwood number, and motile microorganism transfer rate (microbial diffusivity rate) are defined as follows:

Skin friction coefficient:

$$C_f = S_{xr}|_{r=R} \Big/ \rho_f u_s^2 \tag{25}$$

Nusselt number:

$$Nu_x = \frac{-\breve{x}q_w}{k_f\left(\breve{T}_s - \breve{T}_\infty\right)}, \tag{25a}$$

Sherwood number:

$$Sh_x = -D_B\left(\frac{\partial\breve{C}}{\partial\breve{r}}\right)\Big|_{r=R} \Big/ D_B\left(\breve{C}_s - \breve{C}_\infty\right), \tag{25b}$$

Motile microorganism transfer rate:

$$n_x = -D_m\left(\frac{\partial\breve{n}}{\partial\breve{r}}\right)\Big|_{r=R} \Big/ D_m\left(\breve{n}_s - \breve{n}_\infty\right) \tag{25c}$$

Furthermore, skin friction coefficient, rate of heat transfer (Nusselt number), Sherwood number, and motile microorganism transfer rate (microbial diffusivity rate) provide the following outcomes.

Table 3
Grid convergence test for Chebyshev collocation method.

Grid Points N	Max Value of $p'(\vartheta)$	Max Value of $\phi(\vartheta)$	Max Residual Error $\Vert\mathbf{F}\Vert_\infty$	CPU Time (sec)
10	1.8245	0.9832	3.4×10^{-2}	0.21
20	1.8198	0.9854	4.7×10^{-3}	0.37
30	1.8183	0.9861	7.2×10^{-4}	0.68
40	1.8180	0.9863	9.6×10^{-5}	1.02
50	1.8180	0.9863	1.1×10^{-5}	1.47
60	1.8180	0.9863	8.7×10^{-6}	1.95

Table 4
Comparison of $p''(0)$ and $\chi'(0)$ for various Ha parameter.

Ha	$p''(0)$			$\chi'(0)$		
	Gull et al. (Gull et al., 2024)	Imran et al. (Li et al., 2025)	Current result	Gull et al. (Gull et al., 2024)	Imran et al. (Li et al., 2025)	Current result
0.1	1.0051	1.0051	1.0052	3.6814	3.6813	3.6814
0.5	1.1181	1.1181	1.1179	3.6466	3.6466	3.6465
0.7	1.2206	1.2206	1.2205	3.6147	3.6147	3.6145
1	1.4142	1.4142	1.4141	3.5531	3.5531	3.5529

Table 5
Computed values of $Re_x^{-1/2}Nu$ (heat transfer rate) influence in stagnation-point flow problem.

Parameters	Values	$Re_x^{-1/2}Nu$	Interpretation
M	0.2	2.31852	Heat transfer is moderately great at low magnetic strength.
	0.4	2.28311	As *M* upsurges, the heat transfer rate slightly declines due to the resistive Lorentz force which reduces the flow and weakens convection.
	0.6	2.14287	The higher magnetic field value drastically declines the thermal transport rate in the stagnation region.
Rd	2.0	2.14718	At lower thermal radiation, the energy transfer is relatively weak.
	4.0	2.47419	Increasing Rd enhances thermal energy transport due to radiative heat addition to the fluid.
	6.0	2.77869	Increasing radiation drastically increases the thermal boundary layer and increases thermal transport from the surface.
Q	2	2.27338	Heat generation contributes moderately to thermal raise within the fluid.
	3	2.35077	As heat generation upsurges, internal heat generation upsurges the temperature gradient, growing surface heat flux.
	4	2.48723	Larger heat generation rate leads to a greater thermal transport rate near the stagnation point.
Ec	0.2	2.29319	Low viscous dissipation results in better cooling operation.
	0.3	2.24672	As *Ec* upsurges, the conversion of kinetic energy to thermal transport suppresses the temperature gradient close the wall.
	0.4	2.17120	Great viscous dissipation declines the rate of heat transport via retaining heat within the boundary layer.

$$
\begin{aligned}
Re_x^{-1/2}Cf &= (1+2\beta M p(0) p'(0)) \\
Re_x^{-1/2}Nu &= -[(1+\mathrm{Rd})\chi'(0)], \\
Re_x^{-1/2}Sh &= -\phi'(0), \\
Re_x^{-1/2}Sn &= -\xi'(0).
\end{aligned}
\tag{26}
$$

3. Numerical solution

3.1. Chebyshev Collocation method

Step 1: Define variables at collocation points

Let

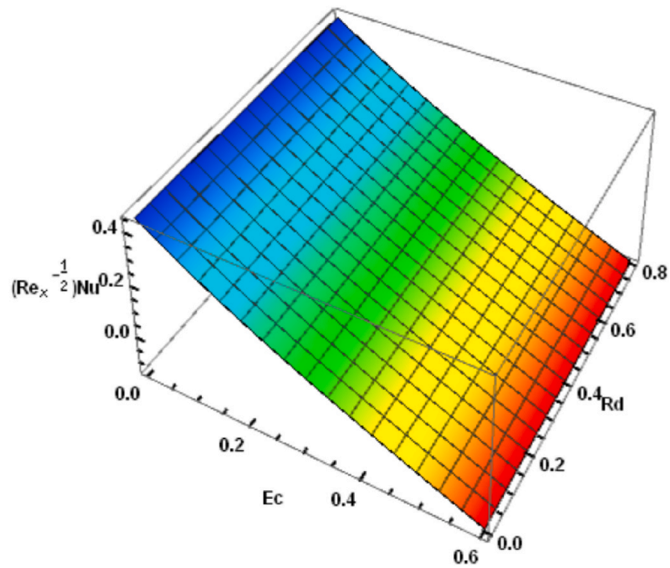

Fig. 1b. 3D plot of Rd on $Re_x^{-1/2}Nu$.

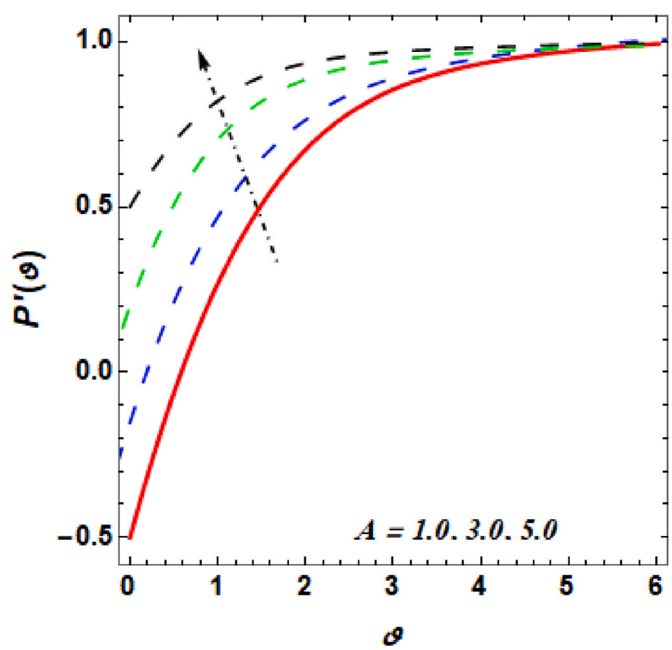

Fig. 2a. Effect of A on the $p'(\vartheta)$.

$$\vartheta_j = \frac{L}{2}(x_j+1) \tag{27}$$

where

$$x_j = \cos\left(\frac{j\pi}{N}\right), j = 0, 1, \ldots, N \tag{28}$$

Step 2: Approximate derivatives

$$p_j' \approx \sum_{k=0}^{N} D_{jk}p_k, p_j'' \approx \sum_{k=0}^{N} (D^2)_{jk}p_k, p_j''' \approx \sum_{k=0}^{N} (D^3)_{jk}p_k \tag{29}$$

Similarly, for all ξ, ϕ, χ.

Step 3: Substitute into each equation

$$(1+2\vartheta_j M)\sum_k (D^3)_{jk}p_k + 2M\sum_k (D^2)_{jk}p_k + p_j\sum_k (D^2)_{jk}p_k - \left(\sum_k D_{jk}p_k\right)^2 + \left(A - \sum_k D_{jk}p_k\right)Ha^2 + A^2 + \alpha(\chi_j - N_r\phi_j - N_c\chi_j) + \ldots = 0 \tag{30}$$

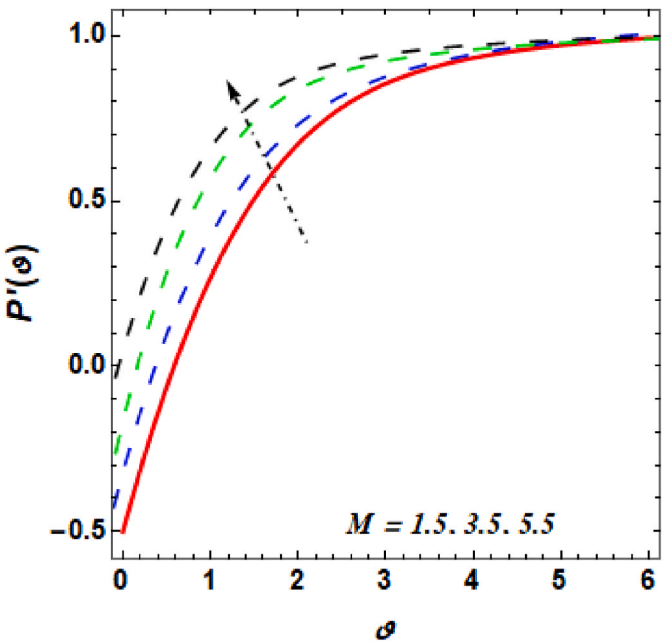

Fig. 2b. Effect of M on the $p'(\vartheta)$.

$$(1+R_d)2M\vartheta_j\sum_k (D^2)_{jk}\chi_k + 2M\sum_k D_{jk}\chi_k + \mathrm{DuPr}\left(\left(1+2M\vartheta_j\right)\sum_k (D^2)_{jk}\phi_k + 2\mathrm{M}\sum_k D_{jk}\phi_k\right) + Q\chi_j + Pr\left(p_j\sum_k D_{jk}\chi_k - 2\sum_k D_{jk}p_k\chi_j + \left(A - \sum_k D_{jk}p_k\right)^2 Ha^2Ec\right) = 0 \tag{31}$$

$$(1+2M\vartheta_j)\sum_k (D^2)_{jk}\phi_k + 2M\sum_k D_{jk}\phi_k + ScSr(1+2Mn)\sum_k D_{jk}\chi_k + 2M\sum_k D_{jk}\chi_k - Sck\phi_j \exp\left(-\frac{E}{1+\delta_0\chi_j}\right) + Sc\left(p_j\sum_k D_{jk}\phi_k - 2\sum_k D_{jk}p_k\phi_j\right) = 0 \tag{32}$$

$$(1+2M\vartheta_j)\sum_k (D^2)_{jk}\xi_k + \frac{\mathrm{Lb}}{M}\sum_k D_{jk}\xi_k - Pe\left(\left(\sum_k D_{jk}\phi_k\right)\xi_j + \left(\sum_k (D^2)_{jk}\phi_k\right)\xi_j + \sigma\sum_k (D^2)_{jk}\phi_k\right) = 0 \tag{33}$$

Step 4: Apply boundary conditions

At boundary points $j = 0$ and $j = N$, apply:

$$\text{At } j = N \text{ (i.e., } = 0\text{)} : p_N = S, p_N' = 1, \phi_N = 1, \chi_N = 1, \xi_N = 1 \text{At } j = 0 \text{ (i.e., } \vartheta = L\text{)} : p_0' = A, \phi_0 = 0, \chi_0 = 0, \xi_0 = 0. \tag{34}$$

For Table 3, it was observed that the maximum values of $p'(\vartheta)$ and $\phi(\vartheta)$ stabilize after $N \geq 40$. The residual error decreases drastically with increasing N, signifying better accuracy. After $N = 50$, convergence is attained, and growing N further offers diminishing returns. The previously published results by Gull et al. (Gull et al., 2024) and Imran et al. (Li et al., 2025) are in good agreement with the values of $p''(0)$ and $\theta'(0)$ presented in Table 4 for different values of Ha. This consistency confirms the reliability of the current results.

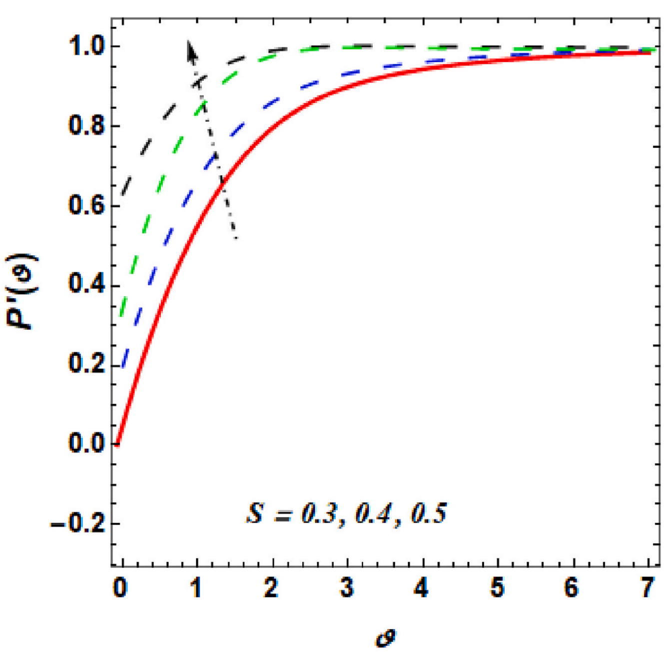

Fig. 2c. Effect of S on the $p'(\vartheta)$.

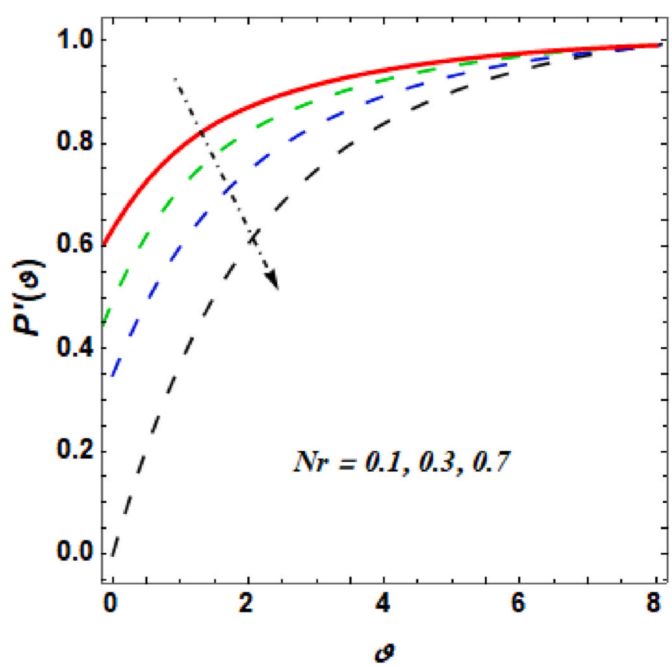

Fig. 2d. Effect of Nr on the $p'(\vartheta)$.

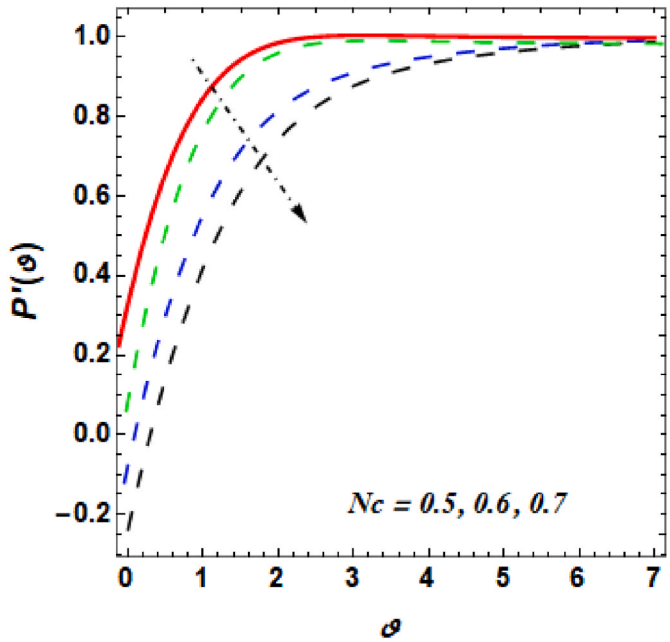

Fig. 2e. Effect of Nc on the $p'(\vartheta)$.

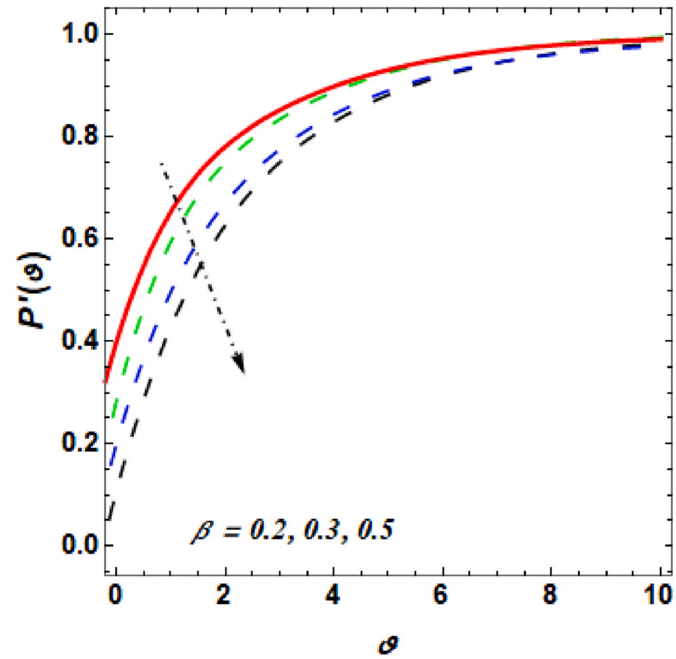

Fig. 2f. Effect of β on the $p'(\vartheta)$.

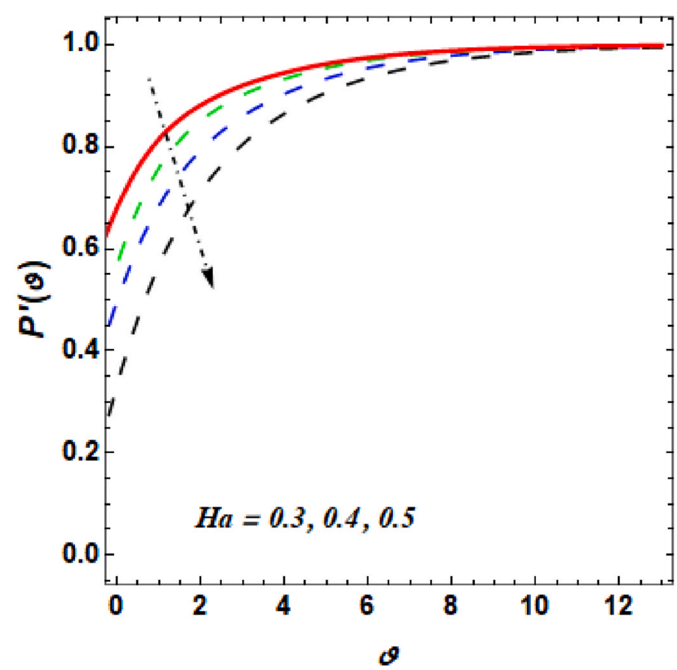

Fig. 2g. Effect of Ha on the $p'(\vartheta)$.

4. Results and discussion

This section presents and analyzes the behavior of velocity, temperature, concentration, and motile microorganism profiles under the influence of key dimensionless parameters for Reiner–Rivlin fluid flow over a stretching cylinder. Table 5 shows calculated values of the local Nusselt number to check the performance of heat transfer in stagnation-point flow of Reiner Riven fluid over a stretching cylinder. The table provides how the various physical parameters affect the thermal transport rate. From Fig. 1b, the Rd shows a positive influence on the $Re_x^{-1/2}Nu$, with greater values of heat transport leading to increased $Re_x^{-1/2}Nu$ Indicating improved thermal energy due to radiative heating.

As the value of velocity ratio increases, the flow velocity increases as seen in Fig. 2a. Physically, as there is a higher velocity jet injected into the slower moving freestream (i.e. the high velocity ratio case), it creates a patch of elevated momentum that strongly perturbs the initial velocity field. This establishes a shear in the boundary of the two flows which increases the mixing rate and momentum diffusion. With an increment in the velocity ratio, the high-speed jet is more likely to enter the primary flow more deeply; thus, creating a velocity profile that is slanted towards the jet axis. This leads to a non-uniform distribution of velocity and larger gradient of velocities, particularly at the mixing interface. It also results in a higher intensity of turbulence because of the increased shear force, creating more complex flows and increasing energy dissipation. As with the jet propulsion systems, the ratio of velocities is an essential factor in optimizing thrust and efficiency of fuel utilized. Velocity ratio has implications on the proper amalgamation of supply air and the room air in HVAC (heating, ventilation, and air conditioning) systems which are directly related to thermal comfort and energy consumption.

Curvature parameter: The influence of curvature parameter on the velocity distribution is shown in Fig. 2b, shows the importance of geometry in fluid dynamic. Curvature parameters are commonly attributed to the extent of the bending or a curve of a streamline or a flow passage and its direct effect is the way the particles of the fluid accelerate, decelerate, and redistribute across the flow domain. With a rise in curvature parameters, i.e. as the flow path becomes more bent or the radius of curvature declines, velocity distribution raises. This asymmetry is because of the effect of centrifugal forces on the elements of the fluid, as this causes pressure and velocity imbalances along the curved part of the flow. Physically, Centrifugal force is therefore produced when fluid flows on a curved surface or through a curved duct pushing the fluid particles outwards toward the center of curvature. It arises due to the force, which exerts pressure in the curved part resulting in a pressure gradient wherein the outer part. This effect is more occurrent as the curvature factor grows bigger (i.e. the curve would be more centered), which results in the development of greater velocity gradients and increases in shear stress at the boundaries.

Suction parameter (S): Fig. 2c displays how the S parameter affects the velocity distribution. This parameter plays an important function in controlling boundary layer performance and flow regulation. It signifies how powerfully liquid is being pulled away from a surface perpendicular to it through a porous wall into the surrounding environment. As the S parameter elevate, the velocity boundary layer increased. In particular, the boundary layer gets thinner, and the velocity profile gets bigger and steeper towards the wall. This causes higher wall shear stress and lower thickness of the boundary layer, and hence the flow is being pulled towards the surface more closely. The physical reason for this behavior is that, that there is an interaction taking place between the suction wall and the momentum of the main flow. The mechanism of suction then is to remove the low momentum fluid up to the near wall of the boundary layer. The removal is efficient in terms that the flow is stabilized by suppressing the development of the velocity disturbances and the delay of the transition between the flows. The capability to regulate the fluid flow through suction has substantial practical applications in both engineering and scientific study. In the aerospace industry, suction is utilized on aircraft wings and turbine blades to stabilize the boundary layer flow. This aids to decrease drag, delay flow separation or stall, and ultimately increases lift and fuel efficiency.

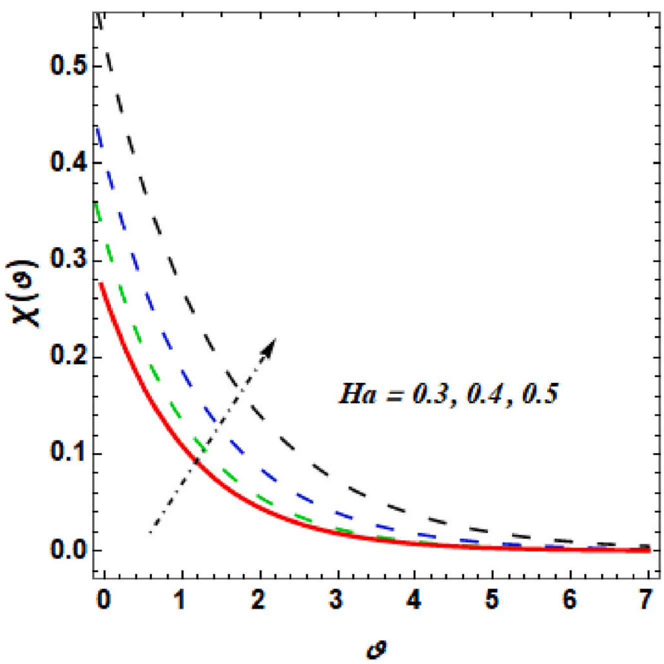

Fig. 3a. Effect of Ha on the $\chi(\vartheta)$.

The Effect of Rayleigh number is display in Fig. 2d, indicates a declining influence of a buoyancy-driven convection in a fluid system. The Rayleigh number is a dimensionless quantity that indicates how strong the buoyancy forces caused by temperature differences are, in comparison to the effects of fluid viscosity and heat diffusion. It is essential in the process of natural convection. High values of Rayleigh number mean that convective motion is strong and dependent on temperature gradient; and low values show the conduction and viscosity effects are strong in restraint of fluid movement. By reducing the Rayleigh number, the strength of the convective currents is reduced thereby resulting in the reduced and flattened velocity distribution within the flow field. The physical explanation of such behavior lies in the base interaction between the forces of buoyancy and resistance in thermally stratified fluid. At high Rayleigh numbers the heating of the fluid adjacent to a hot surface causes large buoyant forces mostly because of the thermal expansion of the fluid resulting in a tendency to rise because hot fluid is now less dense than the cooler flow and would tend to sink. This produces intense circulation and steep velocity gradient especially in the vertical. But as the Rayleigh number is reduced (either by lower temperature differences, greater fluid viscosity or increased thermal diffusivity) these buoyancy forces are not as effective in generating the flow. The effect is that natural convection is stifled, and the fluid moves more slowly, there is less vertical velocity component and less dynamic velocity profile. This can clearly be seen in Fig. 2d, as the Rayleigh number is decreased and the velocity distribution is less, becoming more diffusive. The notion has the utmost practical importance on natural systems and engineered systems.

As shown in Fig. 2e, the buoyancy ratio decreases the velocity, confirming that species-induced buoyancy has a weakening effect on mixed convection flow. The dimensionless number which is the ratio of solutal buoyancy to thermal buoyancy is called the buoyancy ratio. It is the relative measure of strength of density differences due to concentration gradients in comparison to those due to temperature gradients. A reduction in the value of the ratio buoyancy, especially between the

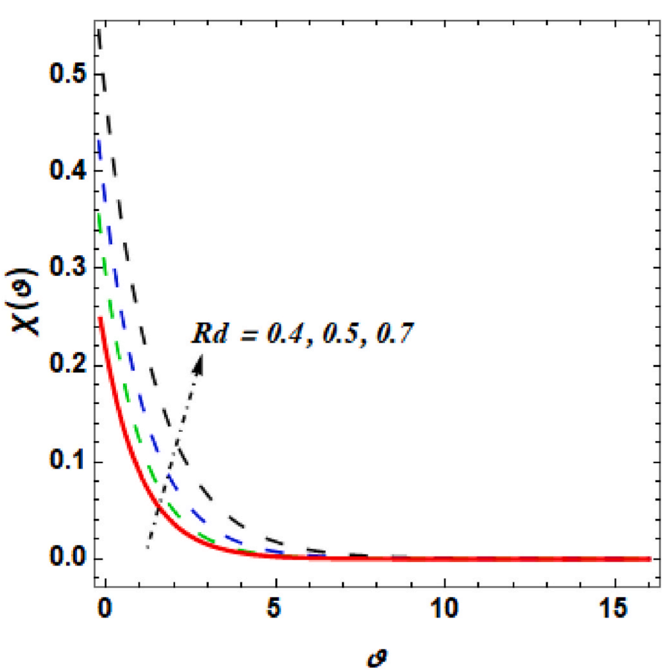

Fig. 3b. Effect of Rd on the $\chi(\vartheta)$.

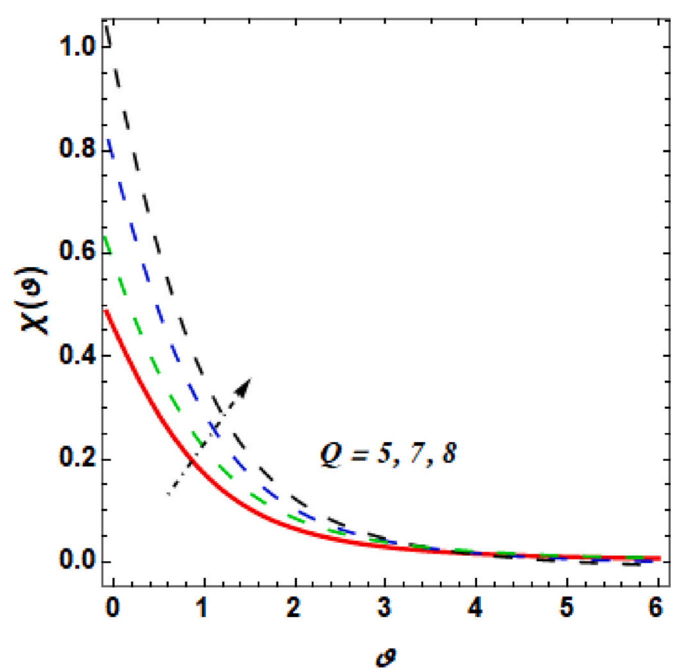

Fig. 3c. Effect of Q on the $\chi(\vartheta)$.

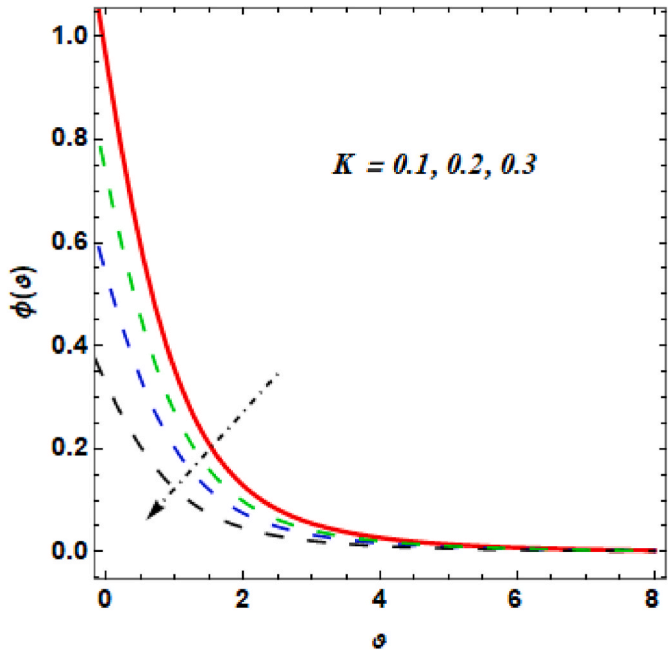

Fig. 4a. Effect of K on the $\phi(\vartheta)$.

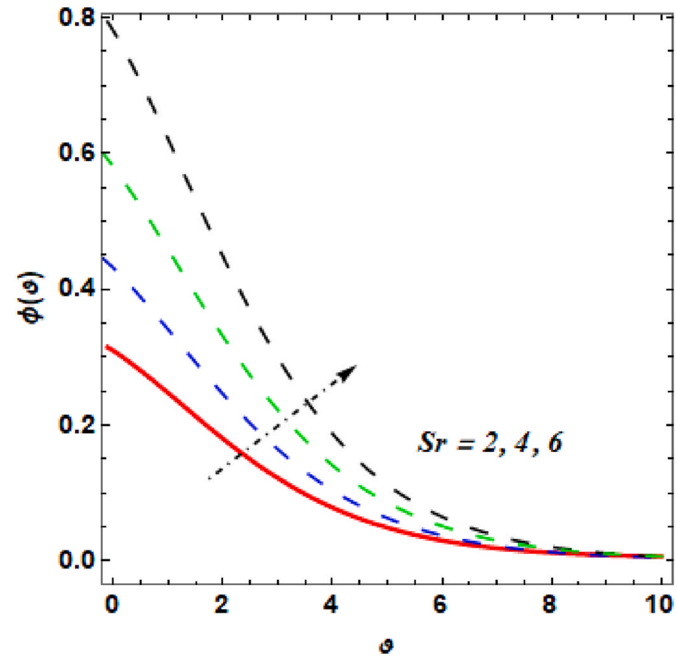

Fig. 4c. Effect of Sr on the $\phi(\vartheta)$.

cases when the ratio value is positive and lower or negative, causes a decrease in the impact of concentration-driven buoyancy. This behavior finds its physical explanation in basic mechanics of double-diffusive convection in which heat and mass transport induce fluid motion. At high buoyancy ratios, the buoyancy caused by concentration differences adds to the thermal buoyancy, which increases the overall upward or downward motion of the fluid according to the gradient's orientation. This phenomenon has huge implications in different practical settings. The concept of buoyancy is therefore vital in many areas of chemical engineering such as reaction and separation process in reactors and distillation columns where flow of products is often critical in enhancing optimality in the purity of products and energy efficiency.

The subsequent phenomenon associated with an increase in value of Reiner-Rivlin fluid variable which affects velocity distribution observed in Fig. 2f illustrates one of the major differences between Classical Newtonian fluid phenomena and the effect of non-Newtonian characteristics of the fluid. Increasing the Reiner–Rivlin parameter enhances the non-Newtonian behavior of the fluid, leading to a decrease in the overall velocity throughout the flow field. Reiner–Rivlin liquids differ from Newtonian liquids since their stresses are not just proportional to the rate of strain but also depend strongly on the deformation fluid. The higher the value of the Reiner-Rivlin variable the stronger these non-linear effects get thus the more resistant the fluid becomes in deformation. The resulting enhanced resistance causes the fluid to be less able to accelerate due to forces that are applied on it and this directly affects the velocity of the flow in the entire flow field.

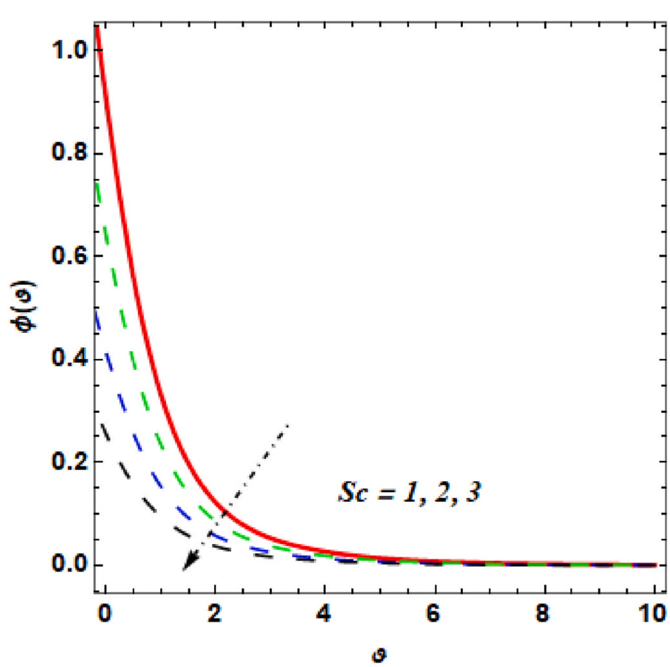

Fig. 4b. Effect of Sc on the $\phi(\vartheta)$.

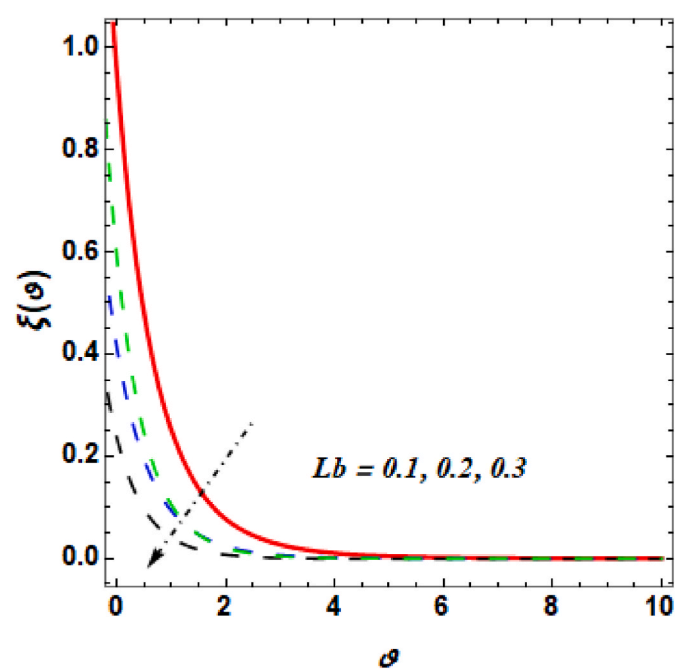

Fig. 5a. Effect of Lb on the $\xi(\vartheta)$.

The effect of increasing the magnetic interaction parameter on the fluid flow, as revealed in Fig. 2g, demonstrates a fundamental principle of magnetohydrodynamics (MHD): the flow of an electrically conducting fluid is affected by the presence of a magnetic field. The higher this parameter the more is the decreased velocity distribution in the fluid and the more is the damp and uniform flow. This is due to the resistive force which the magnetic field introduces into the fluid, namely, the Lorentz force, which acts to prevent the motion of the fluid and hence reduce the flow field. Fig. 3a exemplifies that growing the magnetic parameter raises the fluid temperature. This process is based on the electrodynamic dynamics of a magnetic field interacting with a moving electrically conducting fluid, i.e. a process formed on the laws of magnetohydrodynamics (MHD). The Lorentz force that is thus generated opposes the flow motion; it thereby causes further heating in the form of Joule heating and hence causing a significant rise in fluid temperature. Practically, the behavior plays a critical role in industrial where the MHD effects are present. Also, in nuclear reactor applications such as in cooling systems, MHD is used in the control of heat in coolant loops involving the use of liquid metal coolants that are placed in magnetic fields. The understanding of the role of the magnetic forces on temperature distribution can help design and control systems where heat transfer and electromagnetic effects play functional roles.

The changes in temperature distribution when thermal radiation parameter is increased as shown in Fig. 3b indicates a vital physical process that is vital to the process of heat transfer especially in high temperature surroundings. With an increased value of the thermal radiation parameter, the temperature distribution in the medium increases as well which means that a stronger thermal response emerges. Such an action is based on the basic laws of radiative heat transfer which is more pronounced in applications involving large temperature gradients or high emissive materials. Thermal radiation is physically the aspect through which matter releases energy as electromagnetic radiation based on the temperature it has attained. This radiation adds as an alternative route of heat transport to the conduction and convection effects in a thermal boundary layer. When the curvature parameter is increased, the fluid flow reduces. This behavior is both physically and practically explicable since geometry of a system directly affects manner of convection or conductivity through a given system. Curvature physically adds geometric restrictions that alter the conducting and convective ways of transferring heat. Where geometries are curved, the radius of the roundness also varies the surface area, thereby influencing the heating or cooling gradients. As curvature parameters increase, geometry tends to be more steeply curved and thus the spatial heat dissipation rate changes. The influence of the rising heat generation parameters on temperature distribution as in Fig. 3c shows a principal behavior in thermodynamics: increase in internal heat generation in a medium causes a rise in the total temperature in a system. Such identification is very important in comprehension of thermal behavior in the systems where heat is not just conducted or carried by airflow or convection of external sources of heat, but also generated internally by the effect of physical, chemical, or electrical operations. Physically, this is related as well to the issue of energy conservation and heat transfer principles. Under conditions when there is a continuing production of heat in a body and the rate of dissipation is not equal to the rate of production then an increase in temperature is required to redress the energy balance. This usually causes a maximum temperature at the center of the domain or the area that is farthest away to cooling surfaces.

The influence of chemical reaction parameters on the mass concentration profile shown in Fig. 4a. The chemical reaction parameter describes the rate or the strength of a chemical reaction, rises, and the concentration of the species that react against each other in the system drops. This is strongly evident in Fig. 4a, as an increment in the

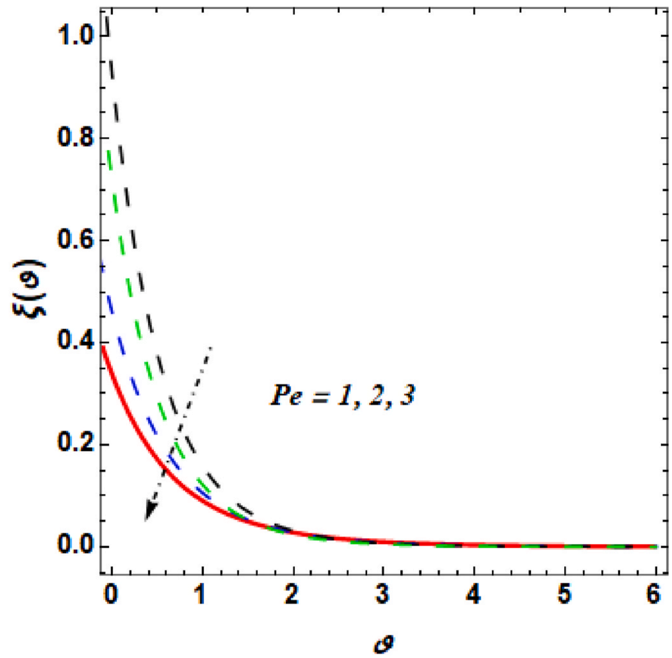

Fig. 5b. Effect of Pe on the $\xi(\vartheta)$.

Parameter of the Chemical reaction leads to a reduction in the mass concentration. Such effect based on the main principles of the reaction-diffusion processes in which the mass movement and the chemical consumption are inseparably connected. Schmidt number is a dimensionless parameter which is calculated as ratio involving momentum diffusivity (kinematic viscosity) to mass diffusivity. Physically, it relates the rate at which momentum is dispersed into a fluid body. The higher the Schmidt number, it means mass diffusion is weak relative to momentum diffusion. These results in a reduced ability of the species to diffuse throughout the medium, leading to a narrower concentration boundary layer and, consequently, a diminished mass concentration profile, as clearly demonstrated in the behavior depicted in Fig. 4b. Physically, the rate at which a substance spreads within a fluid is characterized by the Schmidt number. The influence of the Soret number variation on the mass concentration profile show in Fig. 4c reflects the basic features of mass transfer phenomena involving fluid viscosity and mass diffusivity. Schmidt number is the ratio between momentum diffusivity (kinematic viscosity) and mass diffusivity. The increasing value of Soret number, the greater the momentum is the spread of the momentum compared to that of the mass in the fluid. Fluid inertia means the liquid resists moving and diffusion (due to its thickness or viscosity), a greater Soret number shows that this resistance dominates over the ability of the species to diffuse. As exposed in Fig. 4c, when the Soret number upsurges, the mass concentration becomes more confined and larger close the source or boundary layer.

The Lewis number (Le), which is the ratio of thermal diffusivity to mass diffusivity, is important in transport phenomena, especially in heat and mass transfer systems such as microbial growth on biofilms or in porous media. As the Lewis number decreases, it means mass diffusivity is more dominant than thermal diffusivity. This means, in microbial systems, that the nutrient or substrate upon which the microorganisms must grow can diffuse faster through the medium than heat can transfer (Fig. 5a). Physically, a more dispersed distribution of nutrients, and this will encourage more or longer microbial colonizing of the medium. On the other hand, a higher Lewis number ($Le > 1$) implies that mass diffusion is slower than thermal diffusion, leading to steeper gradients in nutrient concentrations and often causing microbial populations to accumulate in regions with the highest nutrient availability. Higher Pe reduces microbial density profile due to enhanced convective transport, important in microbial fuel cells and bioreactors (see Fig. 5b).

5. Conclusions

This research provides a comprehensive analysis of non-Newtonian stagnation-point bioconvective flow over a stretching cylindrical surface, utilizing the Reiner–Rivlin fluid model. The study integrates the effects of thermodiffusion, bioconvection, and viscous dissipation to thoroughly explore the coupled transport of momentum, heat, and mass. An entropy generation assessment further enhances the understanding of energy losses and irreversibility within the system. The key outcomes are listed below.

- Increasing the velocity ratio enhances the velocity distribution due to stronger momentum coupling. Useful in optimizing flow in biomedical and microfluidic devices.
- Higher curvature increases both velocity and temperature distributions by inducing centrifugal forces, aiding fluid acceleration and thermal mixing in curved microchannels.
- Increased suction elevates velocity by stabilizing boundary layer development, beneficial in filtration systems and biomedical fluid control.
- An increase in Rayleigh number reduces the velocity due to enhanced buoyancy-driven resistance.
- A higher buoyancy ratio decreases velocity distribution by intensifying thermal–solutal stratification.
- Higher magnetic influence reduces velocity by inducing Lorentz forces that resist fluid motion.
- Increases in magnetic effects also raise the temperature distribution due to magnetic heating, significant in MHD thermal systems.
- Reduce the mass concentration profile by consuming species through chemical transformation, relevant in biochemical reactions and drug delivery systems.
- Higher Sc reduces mass concentration due to lower species diffusivity, important in species transport modeling.
- As the radiation parameter (Rd) increases, a substantial enhancement in the fluid temperature is observed across the flow domain.
- Increasing the Soret number raises mass concentration via thermophoresis (temperature-induced mass flux), relevant in thermal diffusion studies.
- Increased Lewis number reduces microbial density by decreasing thermal diffusivity relative to mass diffusivity, applicable in multispecies and microbial interaction systems.

CRediT authorship contribution statement

A.M. Obalalu: Writing – original draft, Validation, Software, Methodology, Formal analysis, Conceptualization. **Ayodeji Felix Isarinade:** Writing – original draft, Validation, Software, Methodology, Formal analysis, Conceptualization. **Umair Khan:** Writing – review & editing, Writing – original draft, Supervision, Resources, Conceptualization. **Aurang Zaib:** Writing – original draft, Visualization, Validation, Investigation, Data curation. **Najiyah Safwa Khashi'ie:** Writing – original draft, Visualization, Validation, Investigation, Data curation. **Dalia H. Elkamchouchi:** Writing – review & editing, Validation, Software, Project administration, Investigation, Funding acquisition, Formal analysis.

Future scope of the study

The future scope of this study includes extending the model to time-dependent and three-dimensional flows, incorporating Carreau, Oldroyd-B, or Powell–Eyring non-Newtonian fluid models, validating the results experimentally, exploring applications in porous media, and integrating machine learning for optimization and predictive analysis.

Data availability statement

The datasets used and/or analyzed during the current study are available from the corresponding author upon reasonable request.

Conflict of interest

There is no conflict of interest.

Acknowledgement

The authors extend their appreciation to the support received from Princess Nourah bint Abdulrahman University Researchers Supporting Project number (PNURSP2025R238), Princess Nourah bint Abdulrahman University, Riyadh, Saudi Arabia.

References

Abbas, A., Hussanan, A., Obalalu, A. M., Kriaa, K., Maatki, C., Hadrich, B., & Kolsi, L. (2024). Effect of non-uniform heat rise/fall and porosity on MHD Williamson hybrid nanofluid flow over incessantly moving thin needle. *Heliyon, 10*(1).

Abhijith, P., Sabu, A. S., Areekara, S., & Mathew, A. (2025). Nonlinear buoyancy driven MHD Reiner–Rivlin nanoliquid flow with quadratic radiation. *Numerical Heat Transfer, Part A: Applications, 86*(9), 2762–2777.

Aich, W., Abbas, A., Martins Obalalu, A., Hassen, W., Said, L. B., Hajlaoui, R., & Kolsi, L. (2025). Double diffusive MHD stagnation point flow of second grade fluid in non-darcy porous media under radiation effects. *Scientific Reports, 15*(1), 395.

Ali, I., Rasheed, A., Anwar, M. S., Irfan, M., & Hussain, Z. (2021). Fractional calculus approach for the phase dynamics of Josephson junction. *Chaos, Solitons & Fractals, 143*, Article 110572.

Anjum, A., Maheswari, C., Lakshmi, B. N., Ramana, R. M., Peerusab, S., & Gaffar, S. A. (2025). Computational study of magnetized 3D revolving hybrid nanofluid with non-linear thermal radiation and heat source/sink over a stretching sheet. *Multiscale and Multidisciplinary Modeling, Experiments and Design, 8*(3), 200.

Anwar, M. S. (2025a). Heat transfer in MHD convective stagnation point flow over a stretching surface with thermal radiations. *Numerical Heat Transfer, Part A: Applications, 86*(10), 3130–3145.

Anwar, M. S. (2025b). Heat transfer in MHD convective stagnation point flow over a stretching surface with thermal radiations. *Numerical Heat Transfer, Part A: Applications, 86*(10), 3130–3145.

Anwar, M. S., Khan, M., Hussain, Z., Muhammad, T., & Puneeth, V. (2025). Investigation of heat transfer characteristics in MHD hybrid nanofluids with variable viscosity and thermal radiations. *Journal of Radiation Research and Applied Sciences, 18*(1), Article 101240.

Cao, F. F., Liu, C. L., Meng, X. L., & Xu, Z. P. (2025). Convective heat transfer parameters in the film cooling with thermal radiation. *Applied Thermal Engineering, 258*, Article 124802.

Cham, A., & Mustafa, M. (2024). Exploring the dynamics of second-grade fluid motion and heat over a deforming cylinder or plate affected by partial slip conditions. *Arabian Journal for Science and Engineering, 49*(2), 1505–1514.

Dharmaiah, G., Goud, B. S., Nisar, K. S., & Reddy, Y. D. (2025). A study of hybrid nano Ag-MgO-H2O flow fluid past a slim needle with thermal radiation and Neild's boundary. *Case Studies in Thermal Engineering*, Article 106328.

Dharmaiah, G., Goud, B. S., Shah, N. A., & Faisal, M. (2023). Numerical analysis of heat and mass transfer with viscous dissipation, Joule dissipation, and activation energy. *International Journal of Ambient Energy, 44*(1), 2090–2102.

Dharmaiah, G., Goud, B. S., Srinivasulu, T., Sridevi, M., & Srinu, A. (2024). Influence of activation energy in steady state hydro dynamic Non-Newtonian nano fluid with mobile microorganisms. *Results in Chemistry, 9*, Article 101653.

Dharmaiah, G., & Shankar Goud, B. (2025). A novel exploration of magnetized nano Jeffrey fluid flow over a chemically reacted permeable disk with ohmic heating. *Modern Physics Letters B, 39*(26), Article 2550121.

Dou, S., Guo, J., Xu, J., Zhang, J., Tian, H., Gan, W., … Yuan, Q. (2025). Small molecule-assisted thermal radiation synthesis of super-sb toward ultrafast and ultrastable sodium storage. *Advanced Energy Materials, 15*(14), Article 2403364.

Eswaramoorthi, S., Nasir, S., Loganathan, K., Gupta, M. S., & Berrouk, A. (2025). Numerical simulation of rotating flow of CNT nanofluids with thermal radiation, ohmic heating, and autocatalytic chemical reactions. *Alexandria Engineering Journal, 113*, 535–550.

Galal, A. M., Benabdallah, F., Bayz, D. A., Ching, D. L. C., Memon, A. A., Abbas, M., & Said, Y. (2025a). Effect of thermal radiation on Marangoni convective flow of ternary hybrid nanofluid with bioconvection and local thermal non-equilibrium effects. *Journal of Radiation Research and Applied Sciences, 18*(2), Article 101378.

Galal, A. M., Elhag, A. B., Khan, Y., Abbas, M., Khidhir, D. M., Kamolova, N., & Abbas, A. (2025b). Thermal analysis of thermo-bioconvection flow of trihybrid nanofluid with oxytactic microbe with heat generation: Applications of nanoparticles and thermal radiation. *Journal of Thermal Analysis and Calorimetry*, 1–16.

Galal, A. M., Obalalu, A. M., Akindele, A. O., Khan, U., Usman, A. A., Olayemi, O. A., & Khashi'ie, N. S. (2025c). Thermal performance of entropy-optimized tri-hybrid nanofluid flow within the context of two distinct non-newtonian models: Application of solar-powered residential buildings. *Computer Modeling in Engineering and Sciences, 142*(3).

Galal, A. M., Saadeh, R., Obalalu, A. M., Khan, U., & Elattar, S. (2025d). Dissipative disorder optimization in the radiative thin film flow of partially ionized Non-Newtonian hybrid nanofluid with second-order slip condition. *Open Physics, 23*(1), Article 20250149.

Galal, A. M., Saadeh, R., Obalalu, A. M., Khan, U., & Elattar, S. (2025e). *Open physics: Dissipative disorder optimization in the radiative thin film flow of partially ionized Non-Newtonian hybrid nanofluid with second-order slip condition*.

Gasmi, H., Obalalu, A. M., Khan, U., Ishak, A., Balogun, A. O., Alessa, N., & Magzoub, O. A. (2025). Irreversibility analysis of the two-phase Non-Newtonian nanofluid model induced by converging/diverging channels with heat source/sink and viscous dissipation effects. *Alexandria Engineering Journal, 123*, 497–510.

Goud, B. S., Dharmaiah, G., Hendy, A. S., & Ali, M. R. (2024). Flow over a stretchable cylinder with nonlinear heat sources/sinks: Magnetic dipoles application. *Case Studies in Thermal Engineering, 54*, Article 104038.

Gull, L., Mushtaq, A., Mehmood, T., & Mustafa, M. (2024). Exploring slip flow of viscoelastic fluid with frictional heating effects: Uncertainty analysis using response surface methodology (RSM). *International Communications in Heat and Mass Transfer, 155*, Article 107548.

Hayat, T., Alsaedi, A., Razaq, A., & Khan, S. A. (2024). HARK formulation for entropy optimized convective flow beyond constant thermophysical properties. *Case Studies in Thermal Engineering, 54*, Article 103983.

Hayat, T., Razzaq, A., Khan, S. A., & Razaq, A. (2024). TASA formulation for nonlinear radiative flow of Walter-B nanoliquid invoking microorganism and entropy generation. *Results in Engineering, 24*, Article 103346.

Huang, Z. Y., Zheng, X. Q., Tan, E. L., Chen, Z. A., Shi, L. H., & Chen, B. (2025). Piecewise calculation scheme for the unconditionally stable Chebyshev finite-difference time-domain method. *IEEE Transactions on Microwave Theory and Techniques*.

Hussain, S. M., Khan, U., & Obalalu, A. M. (2025). Impact of axial electric and inclined magnetic fields on tri-hybrid nanofluid through an electroosmotic flexible pump for biomedical microfluidic devices. *Chemical Physics Impact*, Article 100902.

Imran, M., Zeemam, M., Basit, M. A., Sultan, R., Alharthi, A. M., Souayeh, B., … Aymen, F. (2025a). Exploration of stagnation-point flow of Reiner–Rivlin fluid originating from the stretched cylinder for the transmission of the energy and matter. *Scientific Reports, 15*(1), 6515.

Imran, M., Zeemam, M., Basit, M. A., Sultan, R., Alharthi, A. M., Souayeh, B., … Aymen, F. (2025b). Exploration of stagnation-point flow of Reiner–Rivlin fluid originating from the stretched cylinder for the transmission of the energy and matter. *Scientific Reports, 15*(1), 6515.

Irfan, M., Muhammad, T., Rashid, M., Anwar, M. S., Abas, S. S., & Narayana, P. S. (2025). Numerical study of nonlinear thermal radiation and Joule heating on MHD bioconvection Carreau nanofluid with gyrotactic microorganism's. *Journal of Radiation Research and Applied Sciences, 18*(1), Article 101254.

Jamshidi, M. H., & Arefi, M. (2024). Elastic analysis of functionally graded porous cylinders under uniform internal pressure by using shear deformation theory. *Mechanics of Advanced Materials and Structures, 31*(29), 11393–11412.

John, T. A., & Aderemi, A. K. (2023). The challenges of promoting centripetal forces in Nigeria s sustainable development. *ACU Journal of Social Sciences, 1*(1).

Khan, A., Ahmad, H., Devi, S. U., Farooq, M., Batool, S., & Hussain, S. M. (2025). Significance of melting heat transfer in maxwell nanofluid stagnation point flow across quadratic stratified riga surface. *Results in Engineering, 25*, Article 104456.

Khan, S. A., Hayat, T., & Alsaedi, A. (2023). KHA model comprising MoS 4 and CoFe 2 O 3 in engine oil invoking non-similar Darcy–Forchheimer flow with entropy and Cattaneo–Christov heat flux. *Nanoscale Advances, 5*(22), 6135–6147.

Khan, U., Obalalu, A. M., Zaib, A., Ishak, A., Hussain, S. M., Madhukesh, J. K., … Abed, A. M. (2025). Irreversibility analysis of cross-flow in Eyring–Powell nanofluid over a permeable deformable sheet with Lorentz forces. *ZAMM-Journal of Applied Mathematics and Mechanics/Zeitschrift für Angewandte Mathematik und Mechanik, 105*(2), Article e202300835.

Khan, M., Rasheed, A., & Anwar, M. S. (2023). Numerical analysis of nonlinear time-fractional fluid models for simulating heat transport processes in porous medium. *ZAMM-Journal of Applied Mathematics and Mechanics/Zeitschrift für Angewandte Mathematik und Mechanik, 103*(9), Article e202200544.

Khan, S. A., Razaq, A., Alsaedi, A., & Hayat, T. (2023). Modified thermal and solutal fluxes through convective flow of Reiner-Rivlin material. *Energy, 283*, Article 128516.

Khan, S. A., Razaq, A., & Hayat, T. (2024). SAT formulation for entropy generated hybrid nanomaterial flow: Modified Cattaneo-Christov analysis. *Results in Engineering, 24*, Article 102895, 2024c.

Kumari, M., Kaswan, P., Kumar, M., Lewis, R. W., Oztop, H. F., Singh, N., … Berhanu, M. (2025). Seismic wave reflection characteristics and wave-induced fluid flow in unsaturated porous solid. *Scientific Reports, 15*(1), 1–28.

Li, S., Obalalu, A. M., Kaswan, P., Khan, U., & Balogun, A. O. (2025). Heat transfer mechanism and irreversibility in power law fluid dynamics through converging/diverging channels with radiative effects. *The European Physical Journal - Special Topics*, 1–19.

Mao, Y. Q., Bi, H., Li, X., Chen, K., Wang, Z., Sun, X., & Fu, K. (2025). Twin deformable point convolutions for airborne laser scanning point cloud classification. *ISPRS Journal of Photogrammetry and Remote Sensing, 221*, 78–91.

Mohammed, I. D., Towoju, A. J., & Jamiu, M. S. (2023). Traditional institutions as instrument for rural development in ilorin emirate of Kwara State, Nigeria. *NIU Journal of Humanities, 8*(2), 111–119.

Muhammad, T., & Haider, F. (2025). Time-dependent flow of Reiner–Rivlin nanofluid over a stretching sheet with Arrhenius activation energy and binary chemical reaction. *Multidiscipline Modeling in Materials and Structures, 21*(1), 1–18.

Muhammad, K., & Sarfraz, M. (2025). Regression analysis of squeezing-induced hybrid nanofluid flow in Darcy-Forchheimer porous medium. *Applied Mathematics and Mechanics, 46*(1), 193–208.

Muhammad, K., Sarfraz, M., Alrihieli, H. F., & Elseesy, I. E. (2025). Significance of brownian diffusion and thermophoresis in energy and mass optimization for Newtonian and Non-Newtonian fluid flow. *Case Studies in Thermal Engineering*, Article 106365.

Muhammad, K., Sarfraz, M., Ebaid, A., & Elmannai, H. (2025). Optimization of energy transport via electro-thermal hybrid nanofluid in parallel disks: A Keller-Box simulation. *Chaos, Solitons & Fractals, 198*, Article 116621.

Obalalu, A. M., Khan, U., Alsawah, G. A., & Hussain, S. M. (2025). Features of thermal radiation and tri-hybrid nanofluids in solar-powered tractors using a parabolic trough solar collector with entropy generation effects. *Journal of Radiation Research and Applied Sciences, 18*(3), Article 101801.

Obalalu, A. M., Khan, U., Olayemi, O. A., Zaib, A., Ishak, A., & Sherif, E. S. M. (2024). Thermal transport energy performance on tangent hyperbolic hybrid nanofluids and their implementation in concentrated solar aircraft wings. *Open Physics, 22*(1), Article 20230207.

Obalalu, A. M., Salawu, S. O., Olayemi, O. A., Odetunde, C. B., & Akindele, A. O. (2025). Computational study of bioconvection rheological nanofluid flow containing gyrotactic microorganisms: A model for bioengineering nanofluid fuel cells. *International Journal of Modelling and Simulation, 45*(1), 328–342.

Ogunsanwo, G. O., Alaba, O. B., Obalalu, A. M., Isarinade, A. F., Khan, U., Ghodhbani, R., … Solola, G. T. (2025). Dynamics of second-law analysis and thermal performance in solar-powered tractors using a parabolic trough solar collector filled with tri-hybrid nanofluid. *Journal of Thermal Analysis and Calorimetry*, 1–16.

Oyoru, R. A., & John, T. A. (2022). Impact of corona-virus on the Nigerian public sector; A case Study of the Kwara State civil service. *Lapai international journal of management and social sciences, 14*(2), 44–59.

Puneeth, V., Sarpabhushana, M., Anwar, M. S., Aly, E. H., & Gireesha, B. J. (2022). Impact of bioconvection on the free stream flow of a pseudoplastic nanofluid past a rotating cone. *Heat Transfer, 51*(5), 4544–4561.

Rauf, A., Omar, M., Mushtaq, T., Aslam, S., Shehzad, S. A., & Siddiq, M. K. (2025). Application of artificial neural network in the numerical analysis of Reiner–Rivlin fluid flow with Newtonian heating. *Multiscale and Multidisciplinary Modeling, Experiments and Design, 8*(2), 130.

Razaq, A., Hayat, T., Khan, S. A., & Momani, S. (2023). ATSS model based upon applications of Cattaneo-Christov thermal analysis for entropy optimized ternary nanomaterial flow with homogeneous-heterogeneous chemical reactions. *Alexandria Engineering Journal, 79*, 390–401.

Reiner, M. (1945). A mathematical theory of dilatancy. *American Journal of Mathematics, 67*(3), 350–362.

Sarfraz, M., & Muhammad, K. (2024). Modulation of energy transport in stagnation point flows involving hybrid nanofluids. *Proceedings of the institution of mechanical engineers, part N: Journal of nanomaterials, nanoengineering and nanosystems*, Article 23977914251322202.

Sarfraz, M., & Muhammad, K. (2025). Numerical solutions for thermal and solutal transport of Jeffrey fluid flow subject to rotation via Keller–Box method. *Multiscale and Multidisciplinary Modeling, Experiments and Design, 8*(3), 177.

Sarfraz, M., Muhammad, K., Ahammad, N. A., & Elseesy, I. E. (2025). Synergistic effects of cadmium telluride and graphite nanoparticles with entropy analysis through Keller-box method. *International Communications in Heat and Mass Transfer, 163*, Article 108667.

Sarfraz, M., Muhammad, K., Alrihieli, H. F., & Abdelmohimen, M. A. (2025). Heat and mass transfer analysis in flow of Walter's B nanofluid: A numerical study of dual solutions. *ZAMM-Journal of Applied Mathematics and Mechanics/Zeitschrift für Angewandte Mathematik und Mechanik, 105*(1), Article e202300951.

Shankar Goud, B., & Dharmaiah, G. (2023). Role of Joule heating and activation energy on MHD heat and mass transfer flow in the presence of thermal radiation. *Numerical Heat Transfer, Part B: Fundamentals, 84*(5), 620–641.

Shoaib, M., Naz, S., Raja, M. A. Z., Khanam, R., Ahmad, I., & Nisar, K. S. (2025a). Entropy generation in reiner-rivlin fluid flow under soret and dufour impact: Neural networks applications. *International Journal of Theoretical Physics, 64*(6), 1–30.

Shoaib, M., Naz, S., Raja, M. A. Z., Khanam, R., Ahmad, I., & Nisar, K. S. (2025b). Entropy generation in reiner-rivlin fluid flow under soret and dufour impact: Neural networks applications. *International Journal of Theoretical Physics, 64*(6), 1–30.

Sowayan, A. S., Majeed, A., Khan, S. U., & Riaz, A. (2025). Thermally radiative flow of Jeffrey nanofluid flow for bioconvective flow variable thermal conductivity: PST and PHF analysis. *Journal of Thermal Analysis and Calorimetry*, 1–13.

Venkatadri, K., Rajarajeswari, P., Anwar Bég, O., Ramachandra Prasad, V., Leonard, H. J., & Kuharat, S. (2025). Thermomagnetic bioconvection flow in a semitrapezoidal enclosure filled with a porous medium containing oxytactic Micro-Organisms: Modeling hybrid magnetic biofuel cells. *ASME Journal of Heat and Mass Transfer, 147*(5).

Xu, B., Huang, T., Jing, J., Zhang, C., Li, K., Wang, Y., & Ye, T. (2025). Heat flux distribution and deviation of stagnation point on blunt body under atmospheric dense environment. *Energy*, Article 135007.

Yang, N., Li, Z., Zhang, L., Li, L., Liu, S., Chen, X., … Xu, J. (2025). Full active counter-roller spinning for thin-walled cylinders: Macroscopic deformation mechanism, mesoscopic texture evolution, and forming performance strengthening. *Thin-Walled Structures, 206*, Article 112634.

Yu, L., Li, Y., Puneeth, V., Znaidia, S., Shah, N. A., Manjunatha, S., … Riaz Khan, M. (2025). Heat transfer optimisation through viscous ternary nanofluid flow over a stretching/shrinking thin needle. *Numerical Heat Transfer, Part A: Applications, 86*(3), 518–532.

Zeb, S., Ullah, Z., Albidah, A. B., Khan, I., & Khan, W. A. (2025). The significance of heat transfer through natural convection in stagnation point flow of prandtl fluid. *Results in Physics, 68*, Article 108087.

Zheng, Y., Zhao, W., Song, Q., Ma, C., Yi, Z., Zeng, Q., & Yan, J. (2024). Analysis of solar absorption and thermal radiation properties of a multi-layer structure. *International Journal of Thermal Sciences, 203*, Article 109172.